Report of Investigations No. 226

Production Optimization of Tide-Dominated Deltaic Reservoirs of the Lower Misoa Formation (Lower Eocene), LL-652 Area, Lagunillas Field, Lake Maracaibo, Venezuela

William A. Ambrose, Eulise R. Ferrer[1], Shirley P. Dutton, Fred P. Wang, Antonio Padron[2], Williams Carrasquel[3], Joseph S. Yeh, and Noel Tyler

[1]Lagoven, S.A., Avenida 5 de Julio, Apartado Postal 172, Maracaibo, Edo. Zulia, Venezuela
[2]Formerly with Lagoven; deceased
[3]Formerly with Lagoven

Bureau of Economic Geology
Noel Tyler, Director
The University of Texas at Austin
Austin, Texas 78713-8924

1995

Contents

Abstract 1
Introduction 2
Objective and Study Area 3
Data Base and Methods 3
Geologic Setting 7
Stratigraphic Setting 7
Maracaibo Basin 7
LL-652 Area 7
Structural Setting 8
Maracaibo Basin 8
LL-652 Area 10
Depositional Systems 11
Tide-Dominated Delta Model 11
Distributary Channel 13
Delta Front 13
Tidal Channel and Tidal Flat 13
Transgressive Sand Shoal and Shelf 19
Fluvial-Estuarine Channel 19
Three-Dimensional Facies Architecture 21
Permeability Trends and Diagenetic Controls on Reservoir Quality 22
Reservoir Diagenesis 22
Framework Mineralogy 22
Diagenetic Controls on Reservoir Quality 23
Petrophysical Evaluation 25
Model for Calculating Shale Volume (V_{sh}) 25
Porosity Model (V_{sh}–Porosity Transforms) 25
Permeability Model (Permeability–Porosity Transforms) 27
Water-Saturation Model 27
Cementation and Saturation Exponents 29
Fieldwide Formation Evaluation and Validation by Mapping 29
Net-Pay Determinations 29
Sandstone Architecture and Recovery Optimization of Reservoir Intervals 30
Depositional Controls on Net Pay and SoPhiH 30
Reservoir Examples 30
Upper C-4-X Submember 30
Sandstone-Body Geometry, Lithology, and Depositional Systems 30
Porosity and SoPhiH 30
Net Pay, OOIP, and Remaining Oil 34
Reservoir Development 34

Middle C-3-X Submember 34
Sandstone-Body Geometry, Lithology, and Depositional Systems 34
Porosity and SoPhiH 37
Net Pay 37
OOIP and Remaining Oil 37
Reservoir Development 37
Opportunities and Strategies for Recovery Optimization and Reserve Growth 39
New Extended-Development Locations 40
Resource-Targeted Infill Wells 40
Horizontal and Inclined Wells 40
Secondary Recovery 43
Conclusions 45
Acknowledgments 45
References 45

Figures

1. Average recovery efficiency of oil reservoirs versus depositional systems 2
2. Location of the LL-652 area and Lagunillas field in the Maracaibo Basin and major Eocene stratigraphic sequences in the Maracaibo Basin 4
3. Type log, LL-652 area 5
4. Location of wells, type well, and cored wells, LL-652 area 6
5. Paleotectonic maps showing chronology of Tertiary tectonic episodes in the Maracaibo Basin 8
6. Present structural styles in the Maracaibo Basin 9
7. Fault-bounded compartments in lower Eocene strata, LL-652 area 10
8. Tide-dominated deltaic depositional model of lower Eocene reservoirs, LL-652 area 12
9. Core description of distributary-channel and related facies and net-sandstone map, middle part of the Middle C-5-X submember, LL-3075 well 14
10. Core description of distributary-channel facies truncating delta-front facies, Middle C-3-X submember, LL-3074 well 15
11. Core description of medial delta-front facies, ripple cross-stratified and laminated sandstones, and symmetrical ripples at the crest of the tidal sand ridge overlain by laminated siltstone, Middle C-5-X submember, LL-3075 well 16
12. Core description of distal delta-front facies, Lower C-3-X submember, overlying shelf and transgressive sand-shoal facies, Upper C-4-X submember, LL-3074 well 17
13. Core description of progradational tidal-flat facies and photograph of mud-draped flaser ripples in high-tidal-flat facies, Middle C-4-X submember, LL-2850 well 18
14. Core description of fluvial-estuarine-channel, upper estuarine-channel-fill, and transgressive sand-shoal facies, Lower C-6-X submember, LL-3080 well 20
15. Typical percent-sandstone patterns in offlapping, progradational sequences in the tide-dominated deltaic facies tract, C members, LL-652 area, showing superposition and basinward progradation of distal delta-front, proximal delta-front, distributary-channel and channel-mouth-bar, overlain by lower delta-plain facies 22

16. Average compositional classification of lower Eocene C-member sandstones by facies and by member, LL-652 area 23
17. Porosimeter-measured porosity as a function of present burial depth and quartz cement volume, of C-3-X through C-6-X sandstones, as well as plot of log permeability versus porosity 24
18. Comparison of petrophysical properties between core data and those calculated using porosity values derived from V_{sh}–porosity transforms, C-3-X member, LL-2850 well, and in the C-6-X member in the LL-3080 well 26
19. Comparison of water-saturation values calculated by Indonesian, Simandoux, and Waxman–Smit models and comparison of $V_{sh,}$ porosity and permeability derived from gamma-ray and resistivity logs 28
20. Southwest-northeast stratigraphic dip cross section A–A′ from cores, Upper C-4-X submember, showing permeability variation and basinward thickening of subunit nos. 1 through 4 in the transition from proximal to distal delta-front facies 31
21. Net sandstone, Upper C-4-X submember, LL-652 area 32
22. Maps of reservoir volumetrics, Upper C-4-X submember, LL-652 area, including arithmetic average porosity, SoPhiH, net pay, OOIP, remaining oil, and cumulative oil production 33
23. Net-sandstone-thickness map, Middle C-3-X submember 35
24. Southwest-northeast stratigraphic dip cross section B–B′ and northwest-southeast stratigraphic strike cross section C–C′, Middle C-3-X submember 36
25. Maps of reservoir volumetrics, Middle C-3-X submember, LL-652 area, including arithmetic average porosity, SoPhiH, net pay, OOIP, remaining oil, and cumulative oil production 38
26. Reservoir volumetrics, C members, LL-652 area 39
27. Field extensions in the Middle C-3-X submember 41
28. Map of remaining oil, Middle C-3-X submember, showing proposed new well locations, recompletions, redrilled wells, infill wells, and horizontal and inclined wells for the C-3-X and C-4-X members 42
29. Net-sandstone map, Upper C-4-X submember, east part of field, showing pilot waterflood area 44

Abstract

Structurally complex, heterogeneous, tide-dominated deltaic reservoirs in the Lower Misoa Formation (lower Eocene C members) in the LL-652 area of Lagunillas field in the Maracaibo Basin, Venezuela, have produced 166 million stock-tank barrels (MMSTB) of oil but have a low recovery efficiency of 22 percent. These reservoirs will contain more than 900 MMSTB of unrecovered mobile oil when primary recovery operations at the current 80-acre well spacing end. In this study we characterized lower Eocene reservoirs in the LL-652 area, Lake Maracaibo, to improve estimates of hydrocarbon reserves, to identify potential areas for secondary-recovery projects, and to establish a field-depletion plan to evaluate advanced recovery opportunities and extended development.

A significant remaining oil resource lies in poorly drained or undrained reservoir compartments confined by a combination of complex structure and depositional heterogeneity. Sealing and partly sealing faults, including northwest-trending normal faults and younger north-northeast-trending reverse faults, bound large-scale structural compartments. Stratigraphic heterogeneity is controlled by dip-elongate, distributary-channel, and tidal-ridge sandstones that commonly pinch out over distances of less than 2,000 ft (<610 m). Because these two facies compose most of the reservoir sandstones, they contain most of the remaining oil.

The main control on porosity and permeability distribution in the C members in the LL-652 area is depth. Volume of quartz cement in particular influences reservoir quality, and because volume of quartz cement increases significantly with depth, reservoir quality decreases with depth. Within each reservoir interval, however, depositional architecture controls porosity and permeability distribution. For example, significant permeability contrasts (as much as three orders of magnitude) exist locally between distributary-channel and tidal-flat, fluvial-estuarine channel and distal delta-front, and distributary-channel and delta-front facies, where clay clasts at the base of the distributary-channel facies may retard vertical fluid flow.

Cumulative production varies greatly in each reservoir interval as a result of differences in ages of producing wells, greater-than-average production in areas of repeat section and inferred increased fracture permeability in zones of reverse faults, and differences in net thickness of perforated intervals. The tide-dominated deltaic depositional fabric, however, controls net sandstone and net pay thickness of each reservoir interval and therefore must affect cumulative production.

We made maps of hydrocarbon pore volume (SoPhiH) and remaining oil on the basis of improved petrophysical characterization and production apportioning to specific reservoir horizons by permeability feet (kh). These maps indicate that most remaining oil lies in the poorly developed and structurally complicated north part of the field and where narrow (less than 2,000 ft [<610 m] wide), high-SoPhiH belts are intersected by sealing and partly sealing reverse faults. The original-oil-in-place resource base of the C members in the LL-652 area increased by 867 MMSTB (60 percent) to 2,318.2 MMSTB, mainly in the C-3-X and C-4-X members, by our identifying additional reservoir areas and improving quantification of porosity and other petrophysical parameters. Extended development on the current 80-acre (1,968-ft [600-m]) well pattern that has 97 new wells will increase reserves from 127 to 302 MMSTB. However, 116 MMSTB, in addition to the 302 MMSTB, can be produced from 102 geologically based infill wells strategically targeted to tap areas of high remaining oil saturation in narrow sandstone bodies that pinch out over distances of less than the current well spacing. Horizontal and inclined wells in steeply dipping strata in the C-3-X and C-4-X members can capture additional volumes of poorly contacted mobile oil.

An integrated reservoir-characterization program that includes structural, stratigraphic, petrophysical, petrographic, production-engineering, and volumetric analyses can be used to improve oil-recovery operations in other mature, petroleum-producing provinces of Venezuela where many fields are nearing the first stages of primary depletion. The LL-652 area can serve as a model to demonstrate the most efficient means for recovering the remaining oil resource—a strategy targeting reservoir compartments defined by depositional-facies geometry and structure.

KEYWORDS: Lagunillas field, Lake Maracaibo, lower Eocene, Lower Misoa Formation, reservoir characterization, resource-targeted reservoir development, tide-dominated deltaic reservoirs, Venezuela

Introduction

Many oil reservoirs contain substantial volumes of unrecovered mobile oil that remains trapped in poorly drained compartments after primary and secondary development. For example, of the nearly 500 billion barrels (Bbbl) of oil that has been discovered in the United States, approximately 300 Bbbl will remain unproduced after primary and secondary recovery using current technology (Fisher, 1987; Tyler, 1988). Of this 300 Bbbl, 80 to 100 Bbbl is mobile oil that can be recovered at low cost using conventional infield exploration and development strategies that target untapped compartments and optimize existing waterfloods. Three-dimensional facies architecture and structural complexity strongly control the distribution and continuity of reservoir compartments, paths of fluid flow, and swept areas. Reservoirs that have a complex internal architecture contain large volumes of remaining mobile oil, whereas those that have a simple internal architecture are efficiently drained. The recovery efficiency of reservoirs, moreover, varies tremendously according to depositional type (fig. 1). Homogeneous barrier-island and wave-dominated deltaic reservoirs typically have strong water drives and high mobile-oil recovery, whereas internally complex fluvial-deltaic reservoirs have moderate drive energies and exhibit recovery efficiencies ranging from approximately 20 to 50 percent (Tyler and others, 1984).

The C members of the Lower Misoa Formation in Lagunillas field, Maracaibo Basin, Venezuela, have tide-dominated deltaic reservoirs that are expected to have an ultimate recovery of only 22 percent at the end of primary recovery operations (Tyler and others, 1994). A resource of 923 MMSTB of unrecovered mobile oil is projected to remain in the field at current levels of development using 80-acre well spacing. This report demonstrates that the structural complexity and depositional heterogeneity of these reservoirs have resulted in enormous potential for reserve growth from the remaining mobile oil. The complex, multistage tectonic history of Maracaibo Basin created many structural compartments between intersecting faults of different ages. Sandstone trends, as a result of the depositional architecture, are narrow and linear and oriented consistently northeastward. A preferred pathway for fluid flow exists in these sandstone bodies that are bounded laterally by low-permeability siltstones and mudstones. Additionally, this report documents the volume and location of remaining oil in the C members so that cost-effective, geologically targeted recovery strategies (strategic infill wells, recompletions, and waterfloods) can recover a large part of this resource.

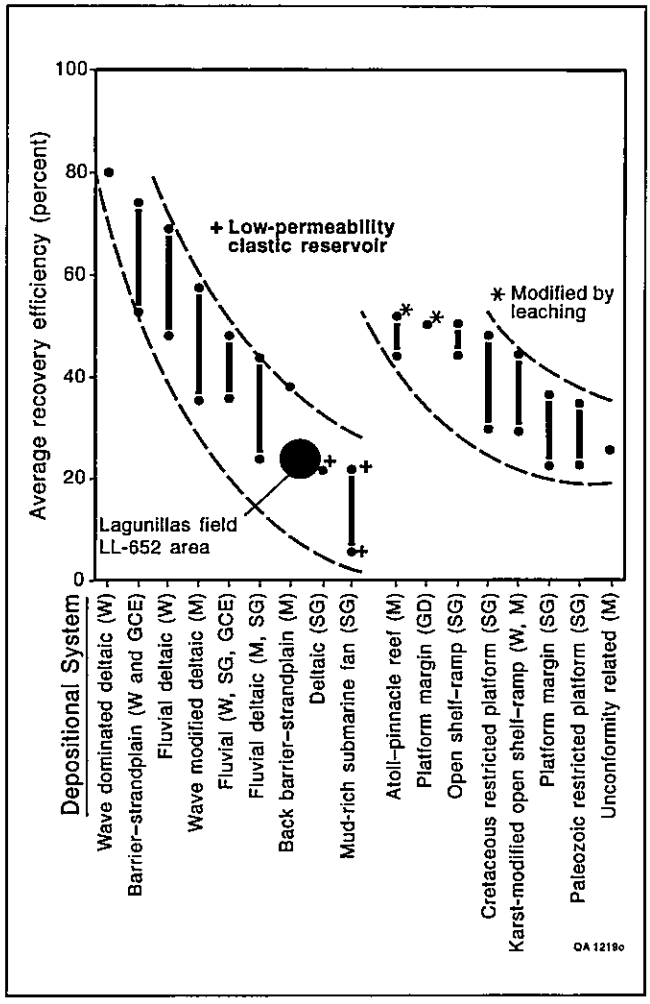


Figure 1. Average recovery efficiency of oil reservoirs versus depositional systems. Lower Eocene tide-dominated deltaic reservoirs in the LL-652 area are expected to have a 22-percent recovery efficiency at the end of primary operations. Abbreviations: W (water drive), GCE (gas-cap expansion), M (mixed), SG (solution gas), GD (gravity drainage). Modified from Tyler and others (1984).

Objective and Study Area

The primary objective of this study was the geological characterization of lower Eocene reservoirs of the Misoa Formation in the LL-652 area, Lake Maracaibo, to improve estimates of hydrocarbon reserves, identify potential areas for secondary-recovery projects, and establish a field-depletion plan to evaluate advanced recovery opportunities and extended development. This objective was met by our conducting an integrated study that included structural, stratigraphic, petrophysical, and production-engineering analyses from well logs, cores, seismic data, thin sections, and petroleum engineering data.

The Maracaibo Basin is one of the most prolific oil-producing basins in the world, containing an estimated 200 billion stock-tank barrels (BSTB) of original oil in place (OOIP). The LL-652 area, discovered in 1953 and one of the leading oil-producing areas in the basin, covers about 54 mi^2 (~140 km^2) and is bounded on the north by the western Tia Juana area and on the west by the Maraven Block 1 concession (fig. 2a). With an OOIP of 1.5 BSTB, during the last 40 yr, the LL-652 area has produced more than 170 million stock-tank barrels (MMSTB) of mainly light oil from the B and C members. Oil is produced from approximately 150 Lagoven wells in 10 reservoirs. Most is produced in the lower Eocene (C-1-X through C-7-X members) in the LL-652 area (135 MMSTB) from the combined C-3-X and C-4-X members (fig. 3). The C-5-X member has produced approximately 18 MMSTB, and the C-6-X member accounts for 7.5 MMSTB. The sandstone-poor C-2-X member has produced 1 MMSTB, the C-1-X member has produced 0.8 MMSTB, and no oil has been produced from the C-7-X member.

A geologic characterization of the LL-652 area was sought by Lagoven to explain controls on production and development problems in the LL-652 area, which include (1) undefined variations in reservoir quality throughout the area, (2) structural complexity in the north, west-central, and southwest parts of the field, (3) poorly documented net-sandstone-thickness trends and their influence on reservoir drainage, (4) unknown or poorly understood reservoir limits along the north and west lease boundaries and in the south part of the field, and (5) discrepancies between, or poor information on, oil–water contacts.

Data Base and Methods

We correlated approximately 20 shale marker beds in the lower Eocene section, representing bounding surfaces of major stratigraphic sequences (fig. 3), in 150 wells in the LL-652 area and 40 wells in Maraven Block 1 (fig. 4). We documented the structural framework using 27 stratigraphic, 22 structural, and 12 seismic cross sections and stratal geometry of major stratigraphic sequences.

Cores from eight wells (fig. 4), which collectively contain 3,266 ft (995.7 m) of section, were described in detail to interpret depositional environments, calibrate log responses, develop a depositional model, and provide a framework for thin-section sampling. Net sandstone from well logs was calibrated to core descriptions using the gamma-ray curve. Net sandstone was initially counted from core descriptions, and then a vertical cutoff line on the gamma-ray curve was drawn in cored intervals to match net sandstone counted from the core descriptions. On the basis of this comparison, we used a 33-percent distance of greatest leftward gamma-ray deflection from a normalized shale base line as a cutoff for counting net sandstone in the C-3-X and C-4-X members. For the C-5-X, C-6-X, and C-7-X members, this cutoff was 28 percent. For logs without the gamma-ray curve (approximately 30 percent of those in the study), resistivity and spontaneous potential (SP) curves were used to measure net sandstone. A depositional model integrated information from core descriptions and net-sandstone, percent-sandstone, and log-facies maps.

Seventy-six thin sections were selected, where possible, at the same depths as core plugs so that petrographic descriptions could be calibrated against core permeability and core porosity. Features described in the petrographic study included mineral composition of grains and clays, cement types, estimates of each type of porosity (primary, secondary, or microporosity), volume of total clay, and diagenetic sequence. We used scanning electron microscopy (SEM) to assess differences in pore types among genetically different sandstones.

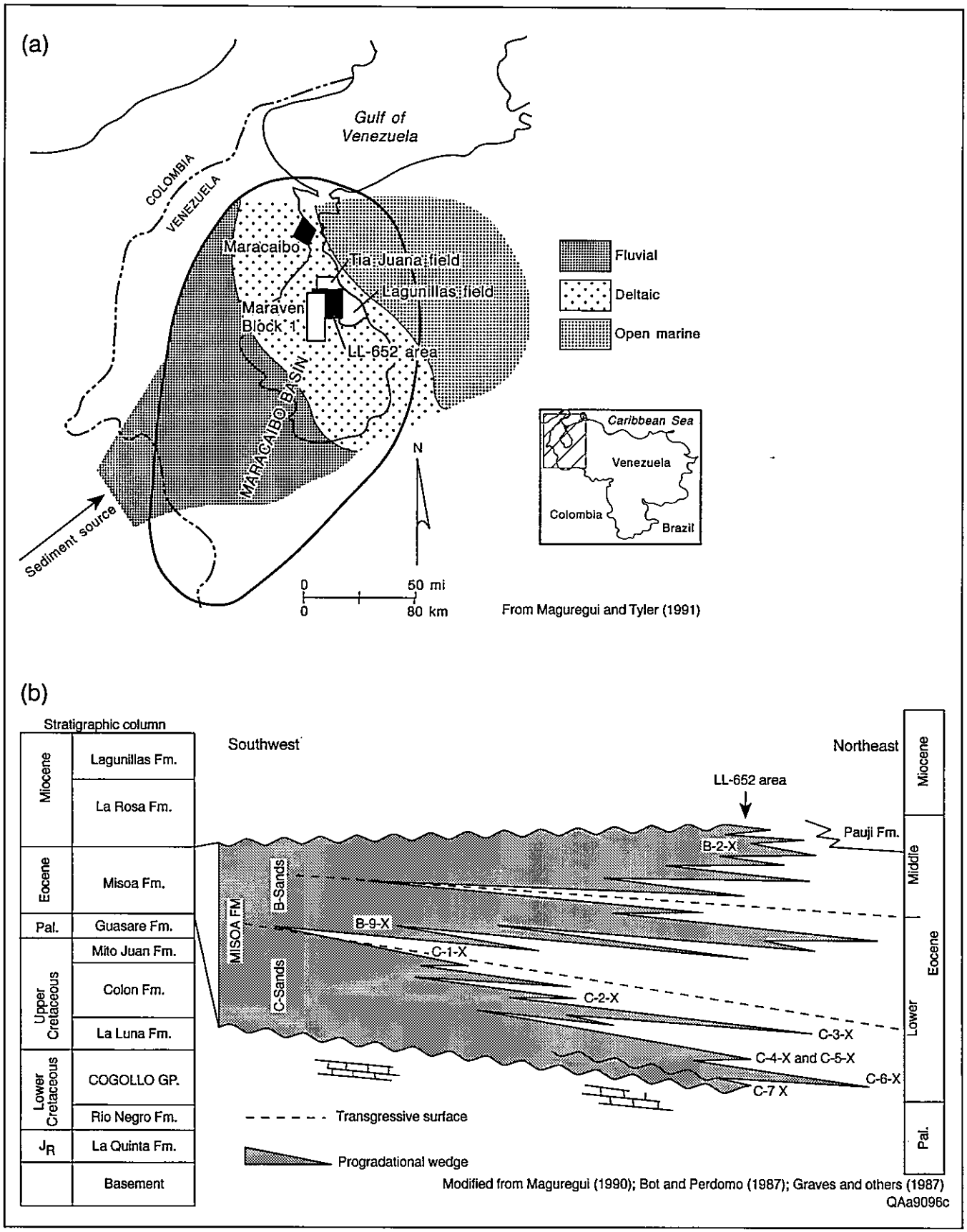


Figure 2. (a). Location of the LL-652 area and Lagunillas field in the Maracaibo Basin. (b) Major Eocene stratigraphic sequences in the Maracaibo Basin.

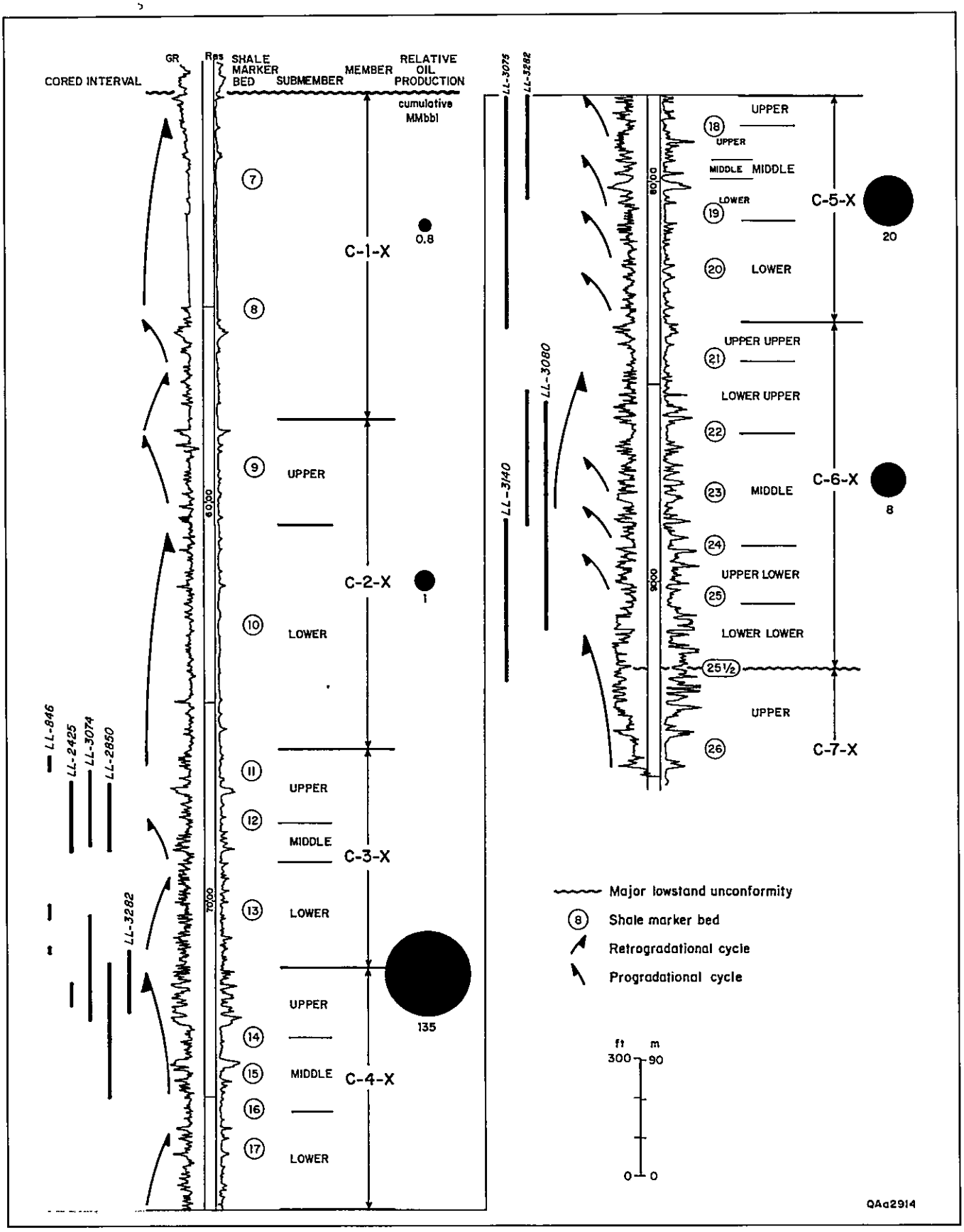


Figure 3. Type log (LL-2942 well), LL-652 area. Size of black dots indicates cumulative oil production in MMSTB. LL-2942 location shown in figure 4.

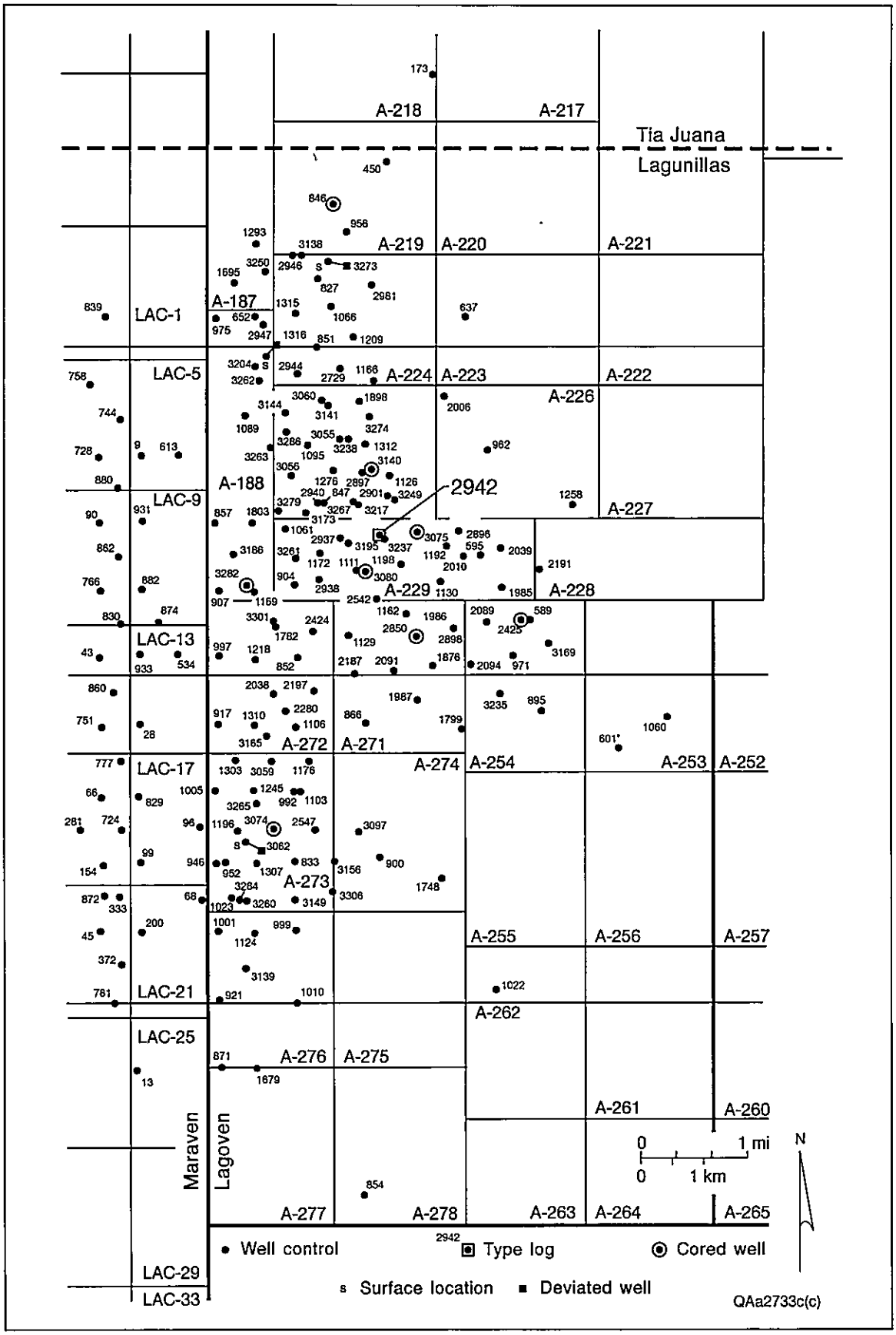


Figure 4. Location of wells, type well, and cored wells, LL-652 area. Type log shown in figure 3.

In conjunction with other structure maps, structural cross sections and fault-surface maps provided a three-dimensional framework of the LL-652 area. Forty-seven dipmeter logs helped us resolve local structural anomalies and complexities. Principal faults were characterized in terms of their possible control on thickness variations in strata, relative age, and seal capacity.

Data from production and pressure analyses were used to infer controls on anomalous production histories and pressures. The stratigraphic horizon of each perforated interval was identified, and producing wells in each member and submember were plotted on structural and stratigraphic maps.

We constructed a petrophysical model by integrating core information, digitized well logs, production data, and key parameters, such as porosity, permeability, V_{cl}, m, n, a, capillary pressure, S_{wirr}, and grain density. Permeability–porosity crossplots were prepared for major reservoir facies identified from cores to characterize the fluid-flow potential. Transform functions relating log response to rock and fluid properties helped us integrate isopach maps of net oil sandstone, porosity, permeability, water saturation, porous hydrocarbon volume (SoPhiH), OOIP, and remaining oil.

Computer-generated maps of water saturation, porosity, permeability, hydrocarbon pore volume (SoPhiH), OOIP, and remaining oil were prepared for each reservoir submember. These maps were then hand-contoured to reflect trends in net-sandstone-thickness and log-facies maps and were later digitized for volumetric calculation. The digitized maps were gridded on 328-ft (100-m) spacing to preserve geological information such as faults, compartment boundaries, and net-sandstone-thickness trends. We constructed SoPhiH maps by multiplying oil saturation (So), porosity (Phi), and net-pay (H) values at each grid point. We calculated OOIP for each submember and structural compartment by integrating the gridded SoPhiH data with area.

A three-step process determined the spatial distribution of remaining oil volume. First, we calculated OOIP per 80-acre well spacing by extrapolating 328-ft (100-m) grids to 1,968-ft (600-m) grids. Second, we partitioned well-by-well production at the submember level, apportioned from permeability feet (kh), among adjacent grids by the reverse-distance weighting method. Third, we prepared maps of remaining oil in place for individual submembers by subtracting oil production from oil-in-place values for each 80-acre spacing grid.

We delineated areas favorable for infill-well development of each reservoir by comparing maps of hydrocarbon volumetrics and production with structural and stratigraphic maps. Specific recommendations for extended development wells, recompletions, and geologically targeted infill locations were made on the basis of these comparisons.

Geologic Setting

Stratigraphic Setting

Maracaibo Basin

The Maracaibo Basin, centered on the southwest margin of Lake Maracaibo, covers approximately 19,300 mi^2 (~50,000 km^2) (fig. 2a). The Cretaceous platform of the basin consists of carbonates and marine mudstones of the Rio Negro to Mito Juan Formations (fig. 2b) (Zambrano and others, 1972; Gonzalez de Juana and others, 1980). Following deposition of the Paleocene Guasare Formation, thick Eocene fluvial-deltaic sediments prograded northeastward on the platform. The lower Eocene, informally referred to as the "C" Sands (Walton, 1967), is composed of a progradational wedge (C-7-X member) truncated by an unconformity associated with a forced regression resulting from an inferred drop in relative sea level and is overlain by several progradational cycles in a net retrogradational succession (Bot and Perdomo, 1987; Graves and others, 1987) (fig. 2b). Maximum transgression in the Maracaibo Basin occurred during deposition of the C-1-X member, and regressive conditions returned with deposition of major progradational clastic wedges of the upper Eocene "B" Sands (Gonzalez de Juana and others, 1980).

LL-652 area

Lower Eocene strata in the LL-652 area are approximately 4,000 ft (~1,220 m) thick (fig. 3). The C-2-X through C-7-X members of the Misoa Formation, informally subdivided by transgressive surfaces into two to three submembers, are bounded by laterally continuous shale marker beds. Submembers range from 50 to 200 ft (15.2 to 61 m) in thickness and contain one or more progradational cycles that

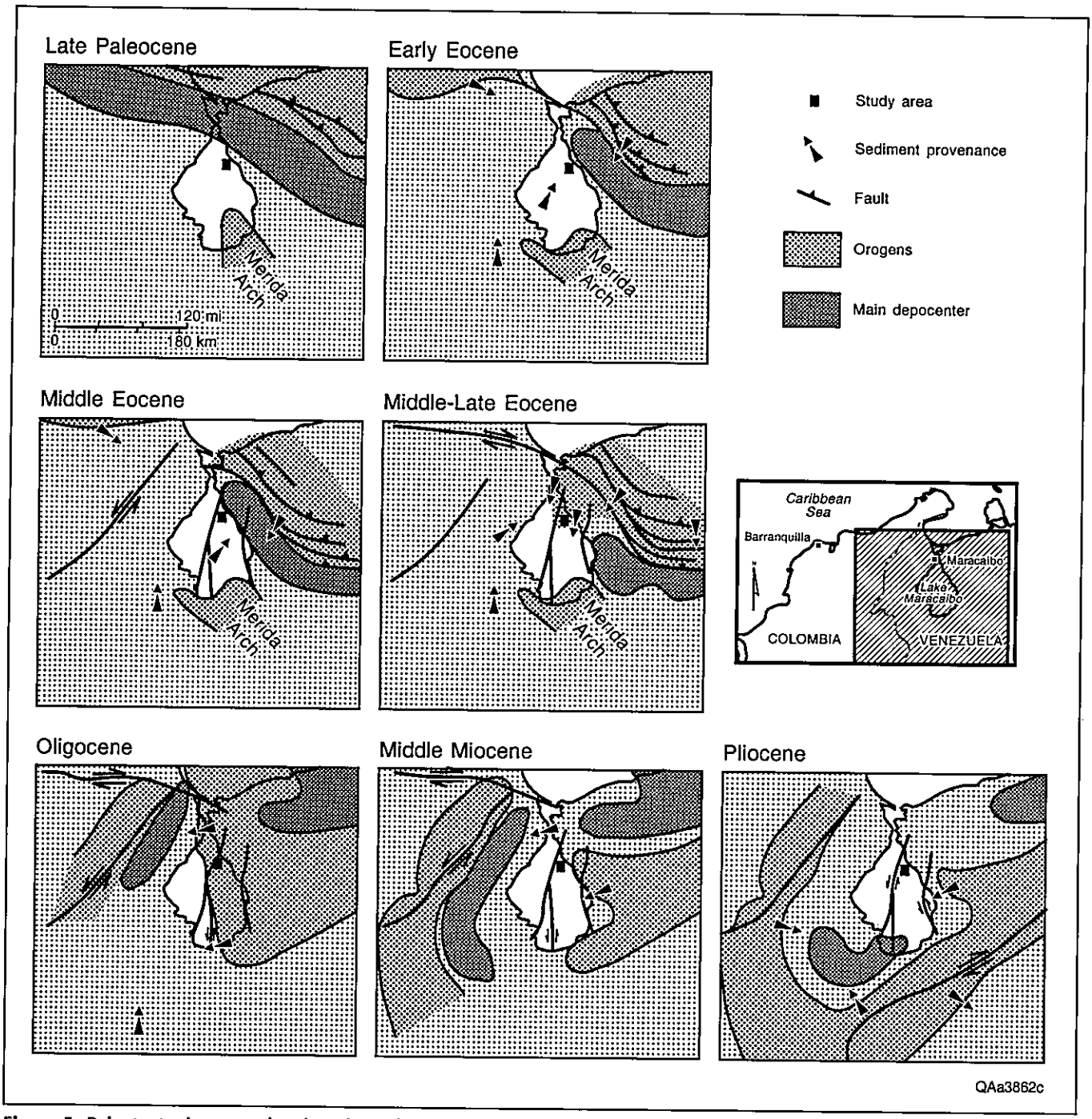


Figure 5. Paleotectonic maps showing chronology of Tertiary tectonic episodes in the Maracaibo Basin. Modified from Lugo (1991).

are each 50 to 80 ft (15.2 to 24.4 m) thick. Beginning with the C-3-X member, a major retrogradational phase characterized deposition of the lower Eocene. The sandstone-rich Middle C-3-X submember represents a brief phase of deltaic offlap, but most sequences in the C-3-X, C-2-X, and C-1-X members are shale dominated and contain thin, volumetrically unimportant sandstones.

Structural Setting

Maracaibo Basin

Multiple tectonic episodes from the Paleocene to Pliocene, reflecting collision of the Caribbean and South American plates, caused several structural trends in the Maracaibo Basin (figs. 5 and 6). North-

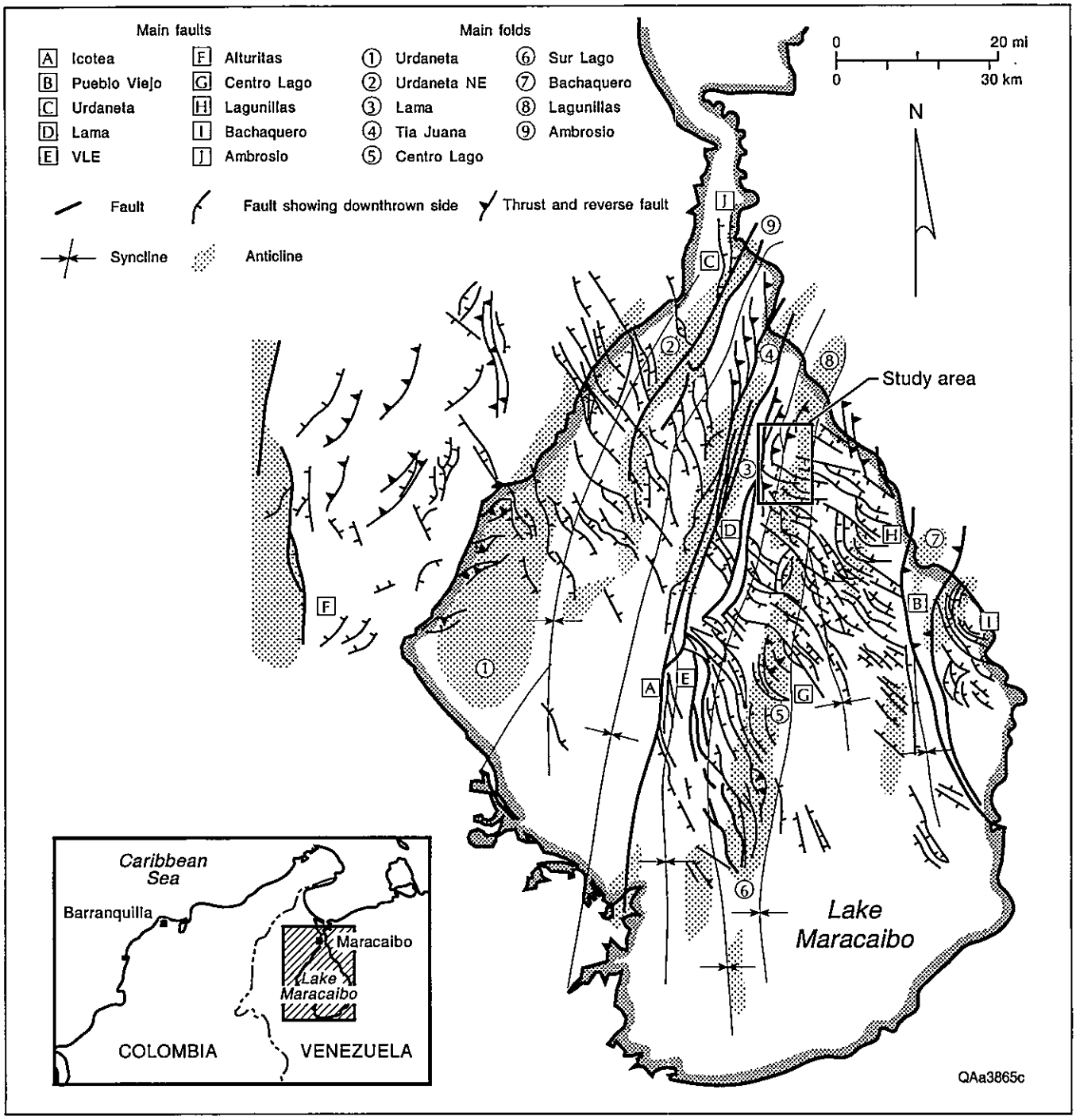


Figure 6. Present structural styles in the Maracaibo Basin. Modified from Lugo (1991).

northeast-trending major faults, repeatedly reactivated during periods of transpression, are mainly represented by the Icotea fault that extends more than 80 mi (>130 km). The Icotea fault (left-lateral strike slip) has associated minor faults in flower and horsetail patterns (Lugo, 1991). The LL-652 area lies in a zone of north-northeast-trending folds that are slightly oblique to the main north-northeast-trending faults. Northwest-trending normal faults offset upper Eocene units and are truncated by the Eocene–Miocene unconformity that resulted from uplift and tilting of the basin during transpression quiescence in early Miocene time. North-trending thrust faults, representing the youngest faulting in the Maracaibo Basin and offsetting all strata, are associated with regional east-west compression in late Pliocene to Holocene

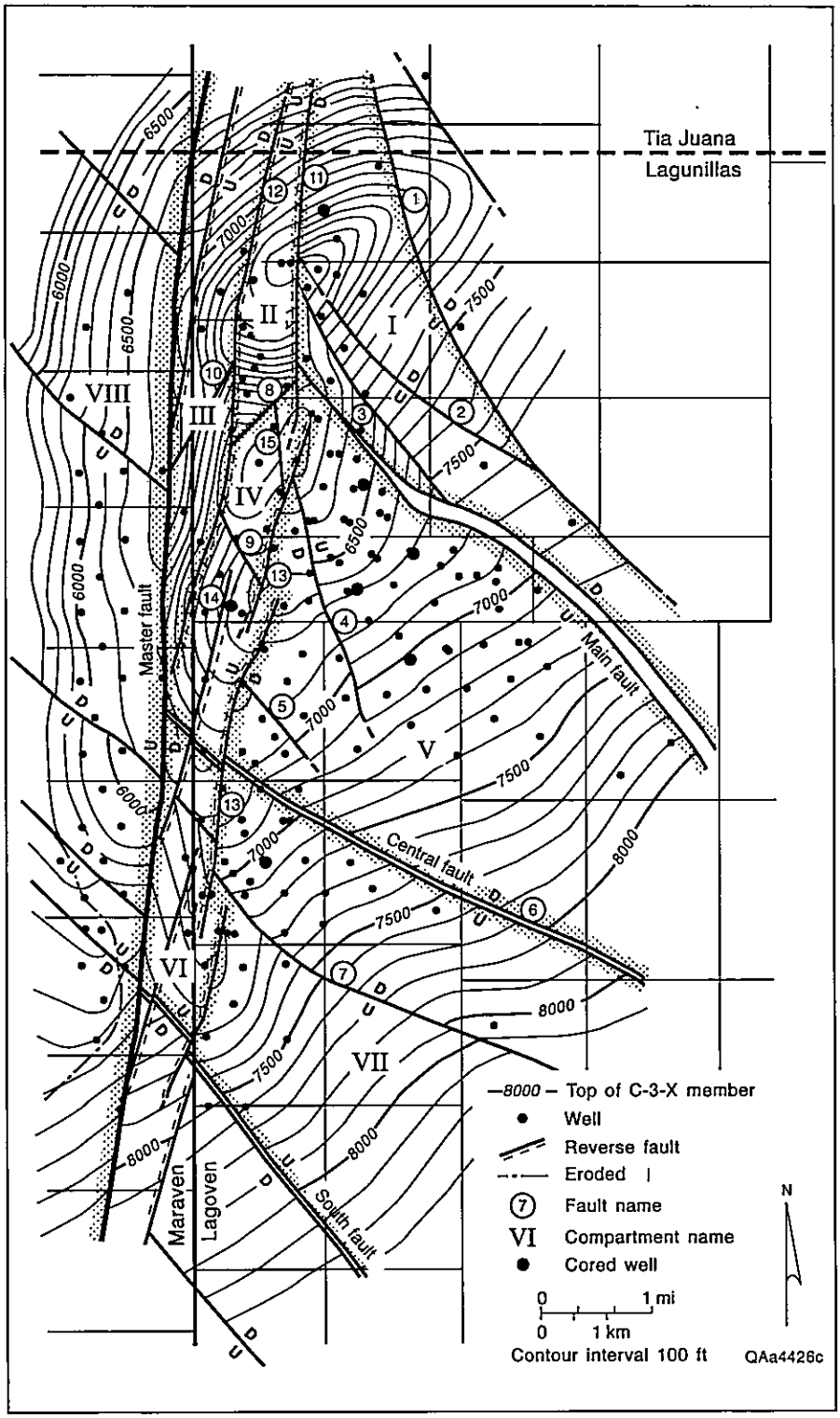


Figure 7. Fault-bounded compartments in lower Eocene strata, LL-652 area.

time. Faults of this type are located in the Centro Lago, Lagunillas, and Bachaquero areas (fig. 6).

LL-652 area

The LL-652 area was affected by multiple tectonic events that generated three trends of normal faults and one trend of reverse faults, representing the local scale of major regional trends defined by Lugo (1991). A major north-northeast-trending normal fault (master fault) on the west margin of the LL-652 area offsets lower Eocene strata by as much as 1,200 ft (366 m) in the south and 800 ft (244 m) toward the north (fig. 7) but offsets the Eocene–Miocene unconformity by only 80 ft (24.4 m). North-northeast-trending folds are represented by an elongate anticline that is slightly oblique to the main north-northeast-trending fault. Normal faults trend northwestward, multiple occurrences of missing section ranging from 50 to 1,200 ft (15.2 to 366 m). Most of these faults offset the entire Eocene section, and they are truncated by the Eocene–Miocene unconformity. A major normal fault (main fault) in the northeast part of the LL-652 area has 400 to 800 ft (122 to 244 m) of throw (fig. 7). North-northeast-trending reverse faults (faults 11 through 14 in fig. 7) displace older normal faults in the LL-652 area. These reverse faults are subparallel to the master fault on the west margin of the LL-652 area and feature repeat section ranging from 60 to 150 ft (18 to 45.7 m) in thickness.

Depositional Systems

Tide-Dominated Delta Model

Sandstone geometry of the C members of the Misoa Formation consists of dip-elongate distributary- and tidal-channel deposits that merge northeastward and that have extensive, dip-parallel delta-front deposits in a tide-dominated deltaic system (fig. 8). Muddy, nonframework facies separating reservoirs consist of lower delta-plain (tidal-flat) deposits that encase distributary- and tidal-channel sandstones and inner-shelf mudstones that in turn encase delta-front sandstones. Seaward (northeastward), delta-front sandstones grade into thinner, distal delta-front sandstones interbedded with mudstones.

The tide-dominated delta model favored for the Misoa Formation is based on (1) diagnostic features in cores, including repetitive, clay-draped reactivation surfaces, abundant clay clasts, and minor occurrences of bidirectional ripples; (2) trends of northeast-trending and -bifurcating sandstone bodies (upward-fining log response) pinching out into muddy deposits (upward-coarsening log response); and (3) a dip-parallel delta-front sandstone geometry. These sandstones are inferred to be marine in origin from burrow types (*Ophiomorpha, Planolites, Asterosoma,* and *Teichichnus*) and from accessory sedimentary features such as symmetrical wave ripples and hummocky cross-stratification.

In contrast to fluvial- and wave-dominated deltaic reservoirs, tide-dominated deltaic reservoirs are characterized by (1) delta-front sandstones that are both dip elongate and dip parallel, (2) sandstones that are heterogeneous because of abundant interbedded mudstone, and (3) (as a consequence of 1 and 2) a low recovery efficiency and, therefore, a high potential for secondary oil recovery. Although delta-front sandstones in fluvial-dominated deltas are primarily dip elongate as in tide-dominated deltas, commonly the delta-front sandstones are not parallel and are flanked by point-sourced, lobate crevasse splay deposits that fill muddy interdistributary areas. In tide-dominated deltaic systems, flood- and ebb-tidal currents rework delta-front deposits into parallel, upward-coarsening sandstone ridges (Off, 1963; Klein, 1970). Although elongate and dip-parallel delta-front sandstones can also occur in fluvial-dominated deltaic systems, where distributaries prograde into lacustrine and interdistributary-bay areas, these types of delta-front deposits are confined to small discrete areas in the lower delta plain. They have a dip-parallel geometry partly controlled by the shape of the oblong lacustrine basin and the bathymetry of the lake floor, rather than by processes in the receiving basin. Additionally, delta-front deposits of the C members have a strong marine association, as inferred from bedforms and burrow types, whereas the modern Atchafalaya lacustrine delta lies in a lower delta-plain setting that has weak marine processes (Tye and Coleman, 1989).

Abundant clay clasts and clay-draped reactivation surfaces in the C members are interpreted to have been caused by repetitive, episodic scouring of a mud-rich substrate by flood- and ebb-tidal currents. Although they occur in a wide variety of depositional settings, clay clasts are abundant in distributary- and tidal-channel deposits and are present as well throughout tidal-sand-ridge deposits in the delta front (Meckel, 1975; Maguregui, 1990; Maguregui and Tyler, 1991). Mud-draped reactivation surfaces that consist of flaser ripples and multiple thin mud layers draping clean, moderately sorted sand indicate high- and low-energy conditions alternating during different phases of the tidal cycle (Reineck and Wunderlich, 1968; Reineck and Singh, 1973). Reactivation surfaces, although not restricted to tidal settings, commonly result from reworking of bedforms by the relatively weak reversing tidal current (Klein, 1970; de Mowbray and Visser, 1984).

Another element recording tidal conditions is bidirectionality of sedimentary structures, such as ripples and crossbeds. Although in cores of the C members, bidirectional ripples are present but uncommon, in many settings in tide-dominated deltaic systems, a dominant tidal current commonly results in unidirectional bedforms being preferentially preserved. The presence of burrows does not exclusively support a tide-dominated deltaic interpretation because they are common in deltaic systems. The wide variety of burrows in all major facies in the C members, however, especially the lower delta plain, indicates a recurring marine influence in a tidal setting.

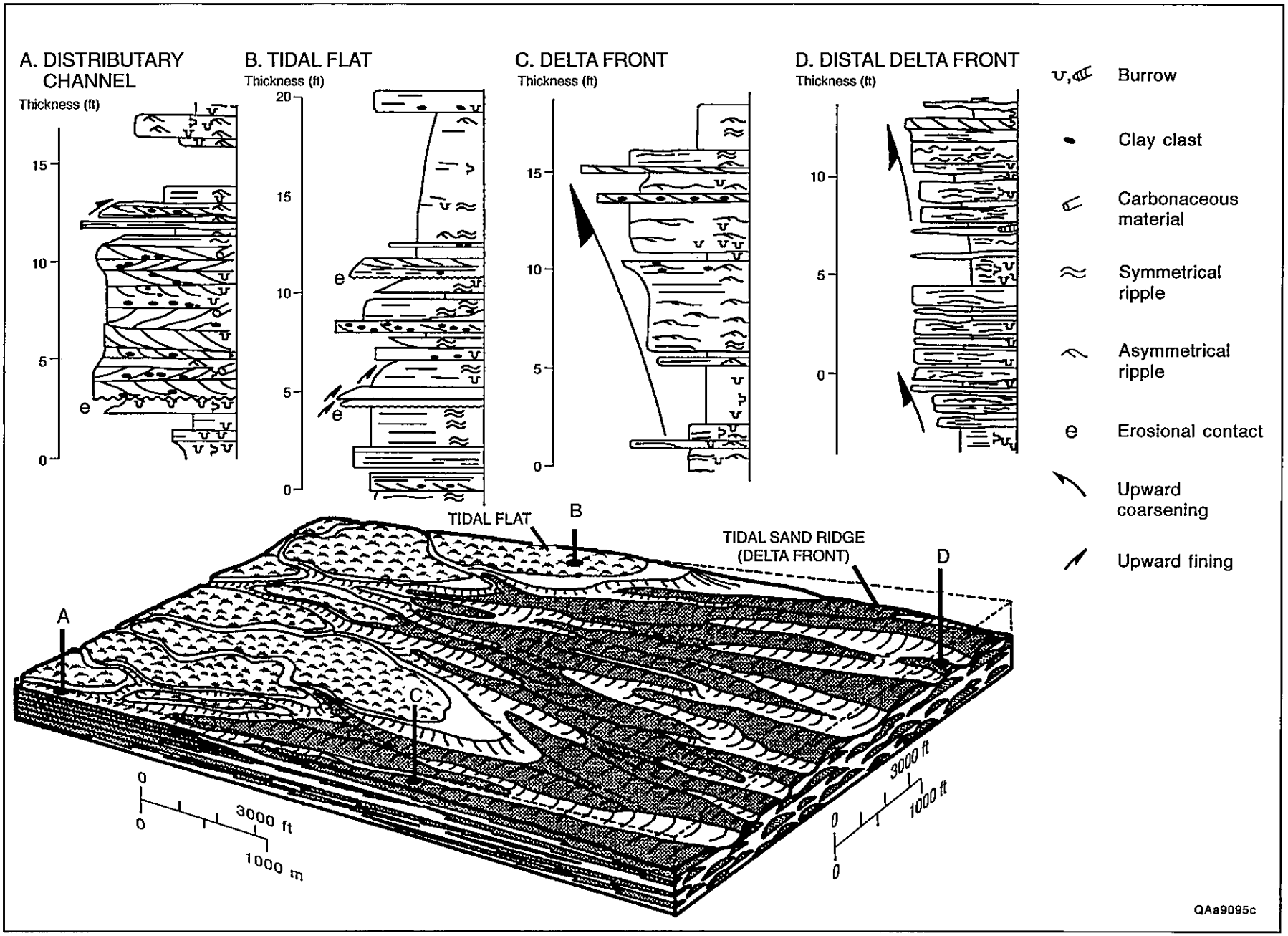


Figure 8. Tide-dominated deltaic depositional model of Eocene reservoirs, LL-652 area. Modified from Maguregui (1990).

Distributary Channel

Distributary-channel deposits in the C members, exhibiting a dip-elongate sandstone geometry and individually ranging from 5 to 20 ft (1.5 to 6 m) in thickness, are erosionally based and upward fining. They typically contain trough crossbeds overlain by asymmetric current ripples and plane beds, and clay clasts and burrows are scattered throughout. An example from the Middle C-5-X submember shows an individual distributary-channel deposit, 13 ft (4 m) thick, that truncates tidal-flat deposits (fig. 9a). This distributary-channel deposit consists of fine sandstone capped by siltstone and very fine sandstone. The lower 9 ft (2.7 m) is extensively cross stratified, whereas the upper 4 ft (1.2 m) is dominated by asymmetrical ripples. Organic fragments, burrows, and very coarse to gravelly clay clasts are present throughout the section. This distributary-channel deposit is part of a narrow (550 to 3,000 ft [168 to 915 m] wide), north-northeast-trending belt (fig. 9b) of more than 20 ft (6 m) of mostly upward fining sandstone bounded by muddy deposits having either upward-coarsening or serrate log responses. These muddy deposits are interpreted to have been formed in a lower delta-plain (tidal-flat) setting transected by a network of distributary channels. The distributary-channel facies commonly truncate delta-front facies. An example from the Middle C-3-X submember in the LL-3074 well (fig. 10) shows a 13-ft (4-m) upward-fining distributary-channel sandstone deposit that truncates a 21-ft (6.4-m) section of upward-coarsening, burrowed delta-front mudstones and sandstones. The distributary-channel sandstone, pervasively rich in gravel-sized clay clasts, contains multiple reactivation surfaces throughout the lower half of the sandstone and a 2.5-ft (0.8-m) zone of calcareous cement at the base, which may have resulted from dissolution of shell lag at the base of the channel. This distributary-channel deposit differs from the previous example in figure 9a, being composed of multiple thin (commonly <1 ft [<0.3 m]) sandstone beds having clay clasts and reactivation surfaces instead of one main sandstone bed. These numerous thin sandstone beds reflect a more distal setting of the distributary channel and deposition by episodic tidal currents.

Delta Front

The delta front is the most volumetrically significant facies in the C members. The delta-front facies is characterized by (1) an upward-coarsening grain-size trend, (2) planar laminae and ripples at the base and small-scale crossbeds at the top, (3) clay clasts and shell debris at the top, and (4) (most significant) a dip-elongate and parallel sandstone geometry.

The proximal to medial delta-front facies ranges from very fine to fine sandstone, commonly more than 20 ft (>6 m) thick (fig. 11a). Sedimentary structures range from crosscutting bidirectional and asymmetrical ripples and multiple siltstone-draped plane beds (fig. 11b) to inclined beds and symmetrical ripples at the top (fig. 11c). Clay clasts are most common at the top of the section. The delta-front deposits are extensively burrowed, *Planolites* and *Ophiomorpha* being common at the top of the section.

Distal delta-front deposits, only 5 to 10 ft (1.5 to 3 m) thick, exhibit a spiky log response. Additionally, the distal delta-front facies includes load structures and slump deposits. The distal delta-front facies in the C members commonly lies in multiple upward-coarsening sequences, each no more than 6 ft (1.8 m) thick, containing load structures and slump deposits (fig. 12).

Tidal Channel and Tidal Flat

Tidal channels are small-scale inlets that transect the muddy tidal flat (fig. 8). In the C members, tidal-channel deposits, typically 5 to 10 ft (1.5 to 3 m) thick and erosionally based, have an upward-fining or blocky grain-size trend. Tidal-flat deposits in the C members are slightly upward fining, reflecting progradation of the muddy tidal flat over the high-energy intertidal sand bar. Tidal-flat deposits are complexly stratified—asymmetrical flaser and symmetrical ripples and plane beds in sandstone are interbedded with mudstone.

Stratification in the lower part of tidal-channel deposits in the C members is poorly preserved, owing to incorporation of channel-margin, bank-collapse deposits. Other important features are microfaults and soft-sediment deformation toward the base and clay clasts that decrease in size upward. A complete tidal-channel–tidal-flat sequence consists of a 10- to 15-ft (3- to 4.5-m), upward-fining section (fig. 13a) having erosionally based, crossbedded and rippled fine to very fine sandstone overlain by siltstone having shale-draped, lenticular flaser ripples that have minor reactivation surfaces reflecting fluctuating depositional energy (fig. 13b).

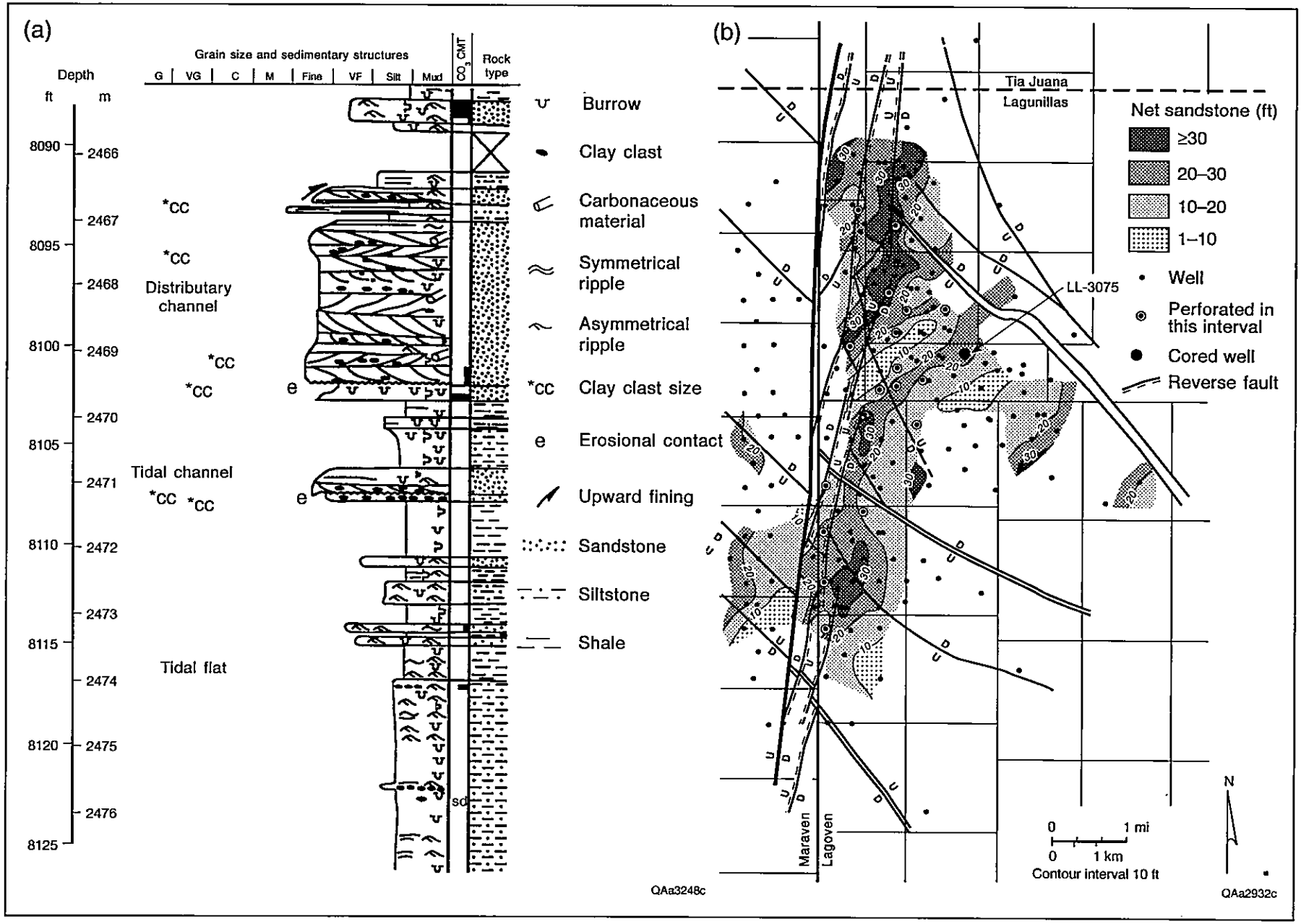


Figure 9. (a) Core description of distributary-channel and related facies, middle part of the Middle C-5-X submember, LL-3075 well. (b) Net-sandstone map, middle part of the Middle C-5-X submember, showing location of distributary-channel facies in cored interval, LL-3075 well.

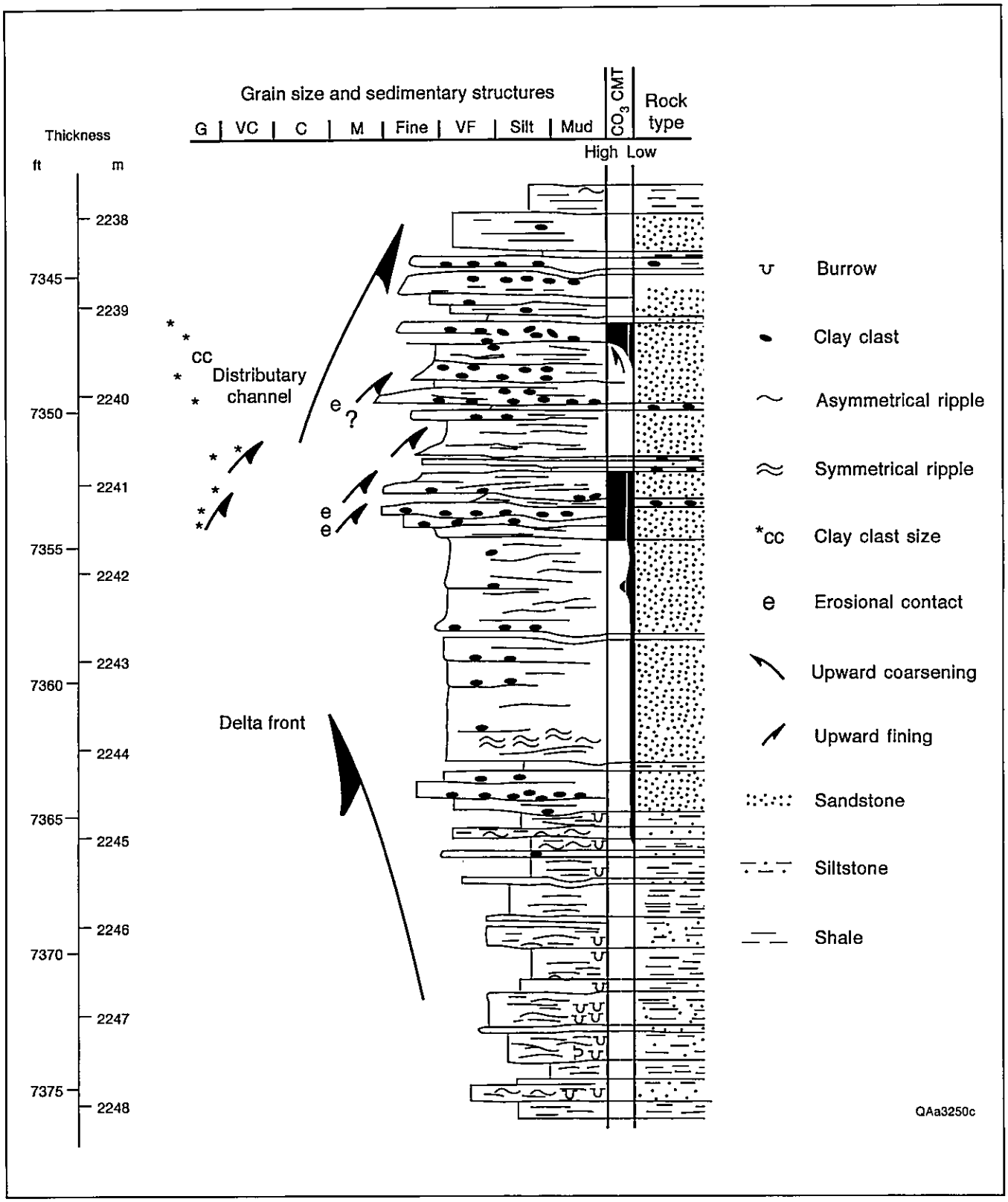


Figure 10. Core description of distributary-channel facies truncating delta-front facies, Middle C-3-X submember, LL-3074 well.

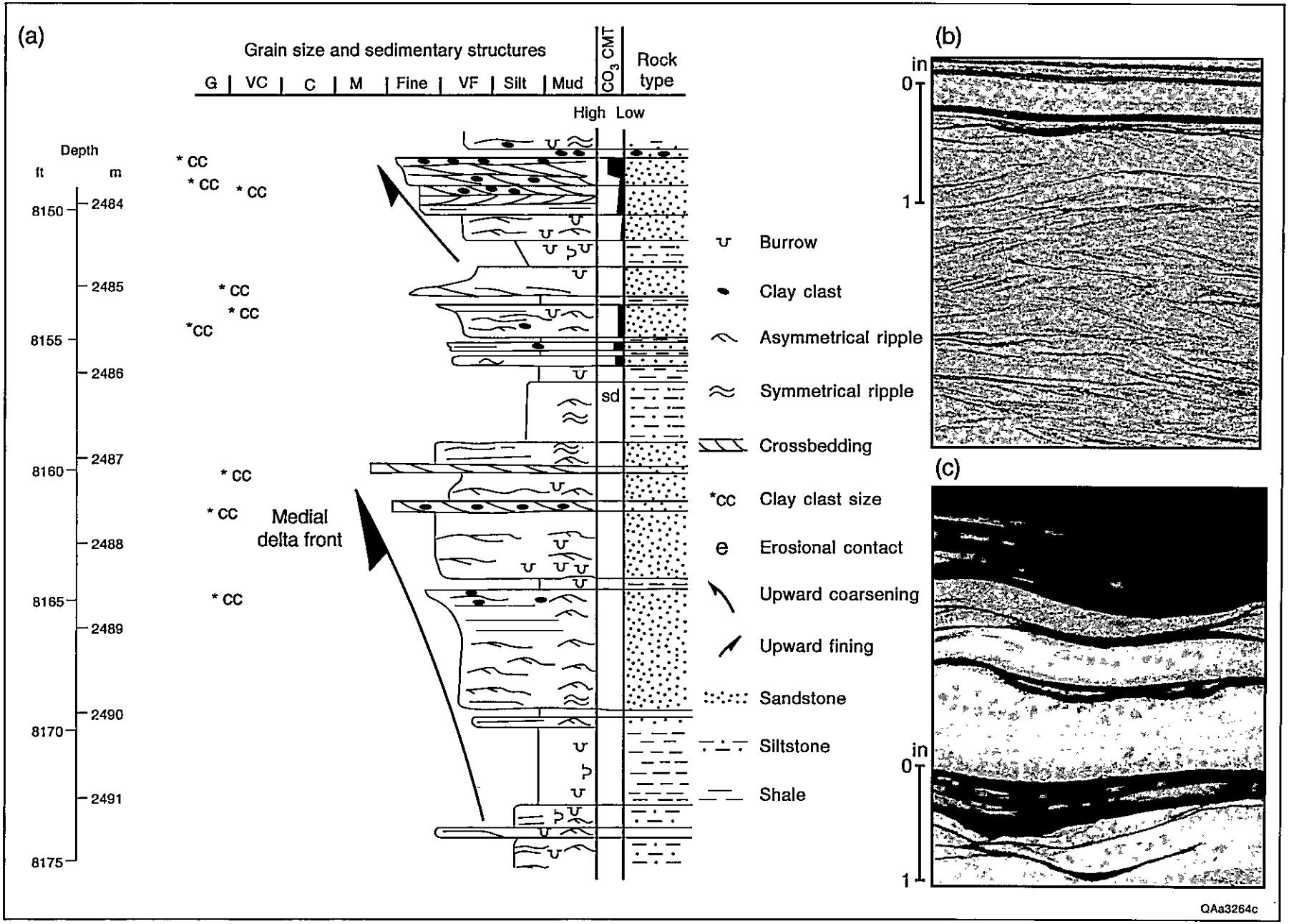


Figure 11. (a) Core description of medial delta-front facies (tidal sand ridge), Middle C-5-X submember, LL-3075 well. (b) Ripple cross-stratified and laminated sandstones, 8,164.5 ft. (c) Symmetrical ripples at crest of tidal sand ridge overlain by laminated siltstone, 8,158 ft.

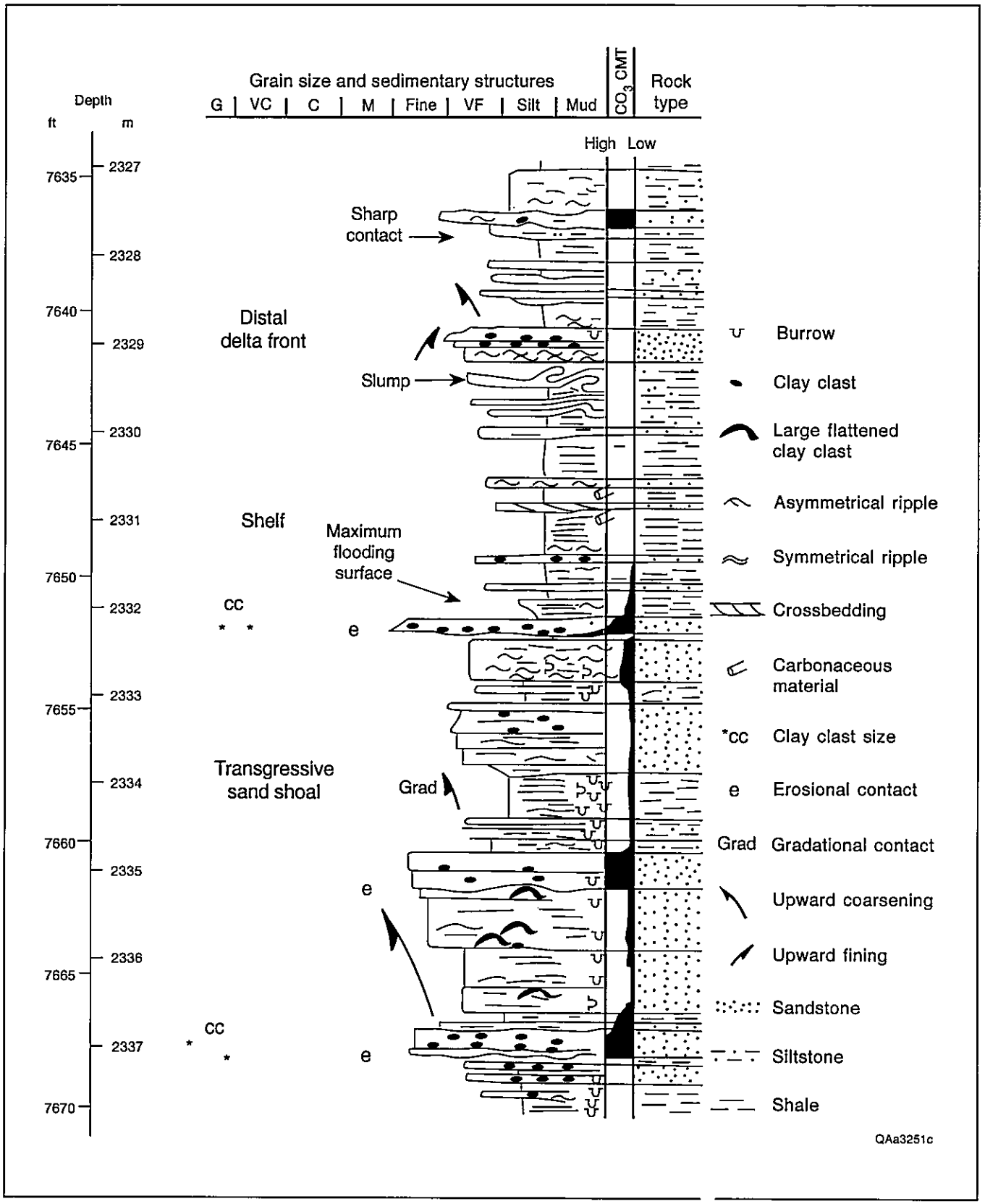


Figure 12. Core description of distal delta-front facies, Lower C-3-X submember, overlying shelf and transgressive sand-shoal facies, Upper C-4-X submember, LL-3074 well. Maximum flooding surface at 7,651 ft (2,333 m) corresponds to boundary between C-3-X and C-4-X members.

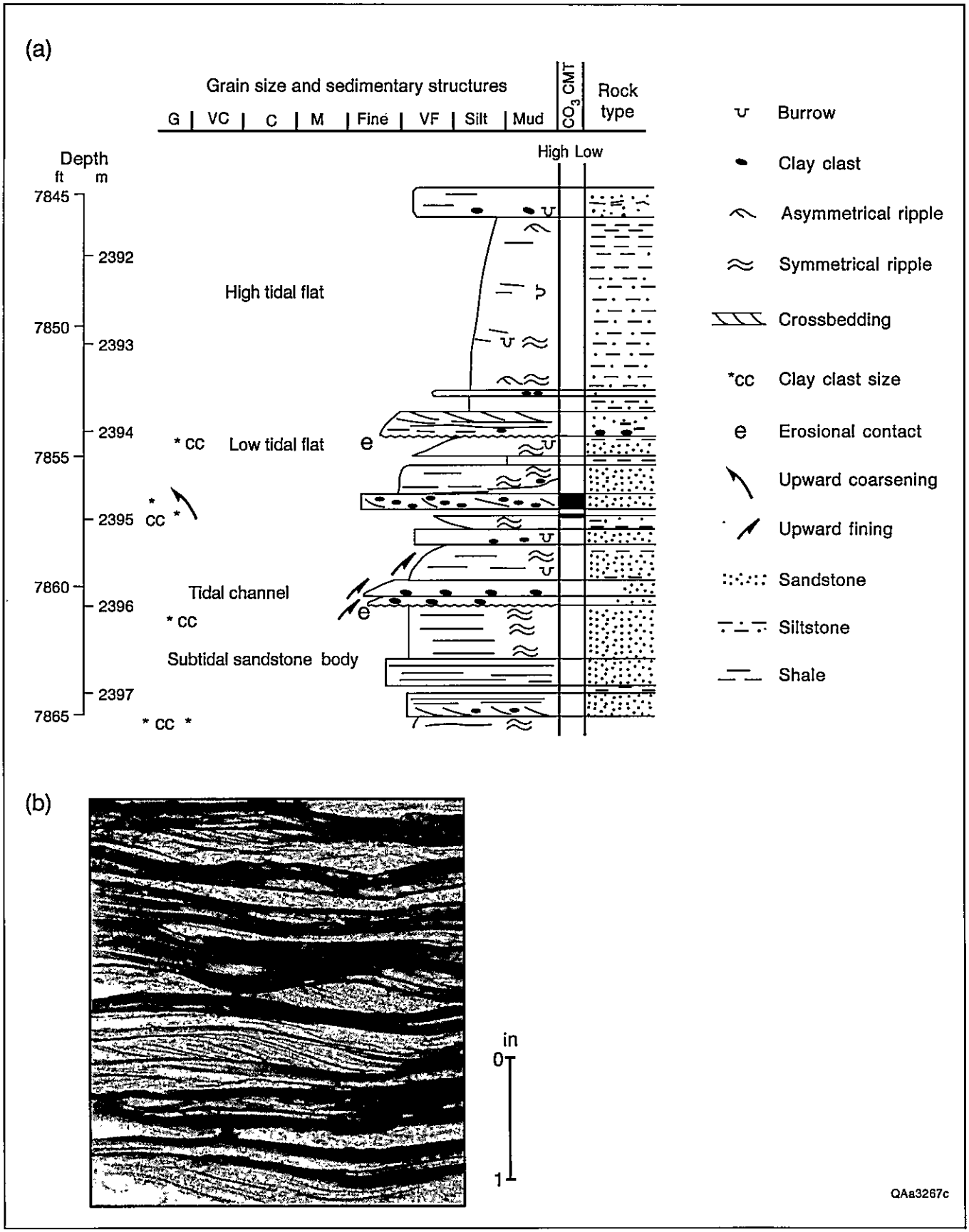


Figure 13. (a) Core description of progradational tidal-flat facies in the Middle C-4-X submember, LL-2850 well. (b) Photograph of mud-draped flaser ripples in high-tidal-flat facies, 7,852 ft.

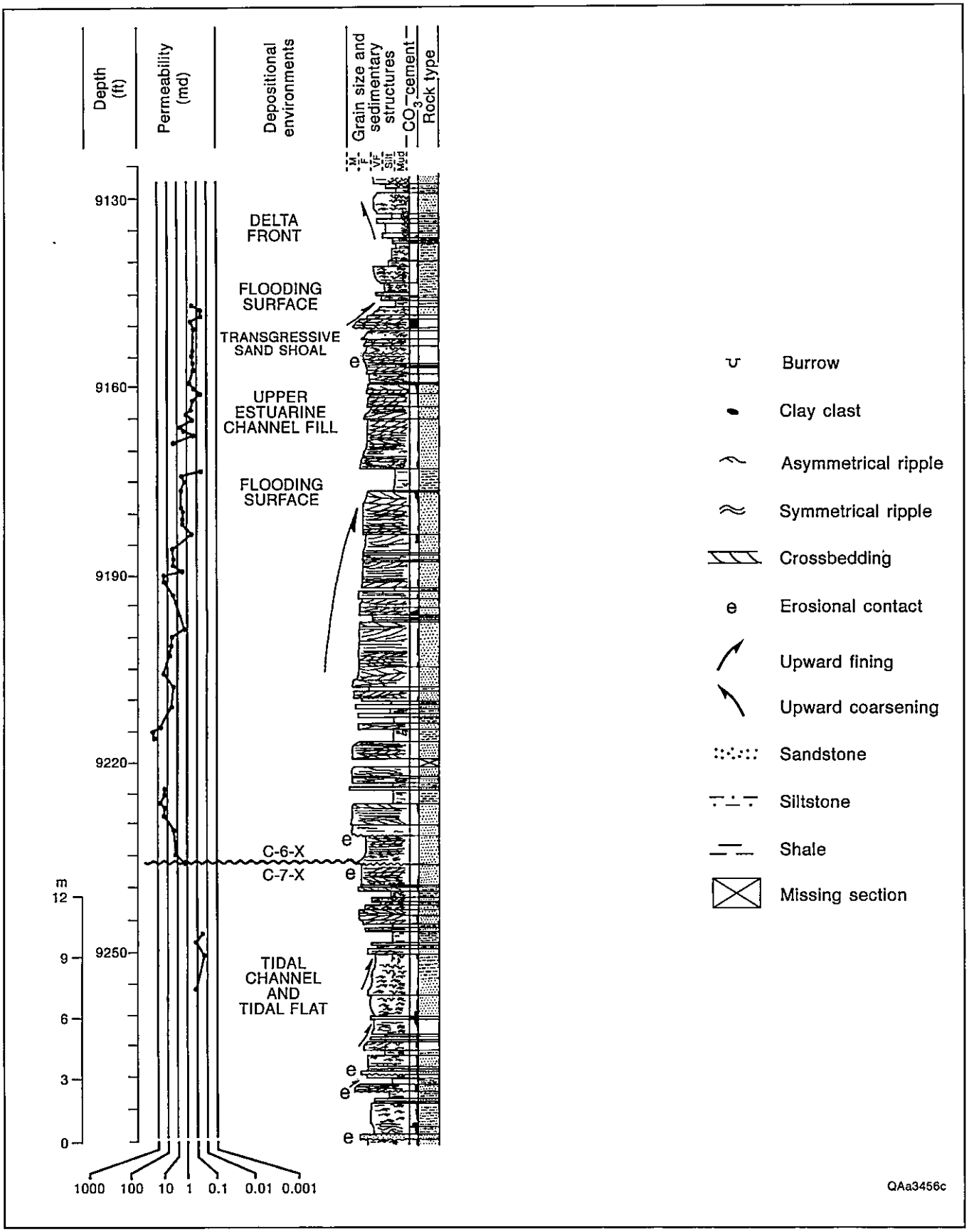


Figure 14. Core description of fluvial-estuarine-channel, upper estuarine-channel-fill, and transgressive sand-shoal facies, Lower C-6-X submember, LL-3080 well. Permeability decreases upward in the sequence.

Transgressive Sand Shoal and Shelf

Transgressive sand-shoal facies in the C members are destructional delta-front deposits distinguished by thin (2 to 10 ft [0.6 to 3 m]), upward-coarsening sandstones having numerous internal erosion surfaces and thin calcareous zones. The shelf facies is characterized by fine grain size, marine burrows, a high degree of lateral continuity, and its stratigraphic position, commonly directly overlying the transgressive sand-shoal facies.

An example of a transgressive sand-shoal–shelf facies couplet (fig. 12) is a 16-ft (4.9-m) complex of multiple upward-coarsening, calcareous sandstones overlain by a 6-ft (1.8-m) section of siltstone having thin (~6 inches [~15 cm]) sandstone interbeds. The lower section of sandstones contains large, irregular, gravel-sized clay clasts; shell fragments; and numerous internal scour surfaces. The shelf facies contains burrowed silty mudstones that have thin lenses of very fine sandstone and siltstone.

Fluvial-Estuarine Channel

Fluvial-estuarine channel deposits in the C-6-X member consist of nonmarine sandstones inferred to have been deposited during a period of major base-level fall. The diagnostic features of the fluvial-estuarine channel facies are (1) an erosional base that commonly truncates marine shale, (2) a lower section of thick, massively crossbedded fluvial sandstone having few or no marine burrows, and (3) an upper heterogeneous section of burrowed sandstones and shales representing estuarine-fill deposits.

An example of fluvial-estuarine-channel-fill sandstone (fig. 14) shows erosionally based, upward-fining sandstone in the Lower C-6-X submember that truncates burrowed marine siltstone and sandstone in the underlying C-7-X member. Permeability and inferred reservoir quality are highest at the base, consisting of unburrowed sandstone that has tabular crossbeds; higher in the section small tabular crossbeds are overlain by ripples and plane beds. Clay clasts and organic fragments, which decrease in size upward, are abundant in the lower part of the fluvial section. The upper section contains multiple burrowed siltstone beds and crossbedded estuarine tidal-channel(?) sandstones. Upward-coarsening delta-front deposits occur at the top of the sequence, which is marked at 9,145 ft (2,788 m) by an inferred flooding surface that overlies a calcareous transgressive sand-shoal deposit (fig. 14).

Similar successions of rock types and bedforms, with variations that mark differences in the timing and relative importance in transgressive and high-stand phases, occur in examples of both ancient and recent valley-fill deposits. A Middle Jurassic valley-fill sequence in northeastern England is inferred to have resulted from a relative sea-level drop, and it subsequently filled during an incremental sea-level rise (Eschard and others, 1991). The sequence consists of basal valley fill of massively crossbedded, erosion-based fluvial sandstone overlain by thinner and lenticular mixed fluvial-tidal sandstones that are in turn overlain by estuarine sand-flat deposits and transgressive shales. These rock types correspond to a three-stage infill of (1) fluvial-dominated straight channels, (2) tidally influenced meanderbelts, and (3) a mixed fluvial-tidal meanderbelt system. As in the LL-652 area, the most permeable sandstones are found in the basal fluvial prism consisting of stacked channel-fill sandstones.

Another ancient valley-fill example lies in the Lower Cretaceous Crystal–Viking field in Alberta, Canada, where estuarine deposits locally truncate shoreface sandstones, resulting in multilevel reservoir compartments (Reinson and others, 1988). The locally occurring valley-fill reservoir sandstone bodies, consisting of multiple depositional units and corresponding to successive channel-fill and estuary-fill deposits, collectively attain a thickness of as much as 100 ft (30.5 m). Unlike the lower valley-fill section in the LL-652 area, corresponding sections at Crystal–Viking field contain no fluvial deposits, but rather tidal-channel and estuarine–bay-fill deposits, suggesting that the incised valley was a site of sediment bypass and that fluvial deposits accumulated downdip of the field. The tidal-channel facies consist of fine- to medium-grained sandstones and conglomerate, forming the primary reservoirs in the valley-fill sequence. Estuarine–bay-fill facies, defined by relatively heterogeneous rock types (interbeds of mudstone and fine-grained sandstone), compose secondary reservoirs locally, where they contain thick sandstones encased in mudstone. The upper transgressive systems tract in Crystal–Viking field is thin and represents nonreservoir facies.

In contrast to valley-fill deposits in the LL-652 area, which have stacked channel fills, recent valley-fill sequences in the Gironde Estuary, France, contain a

basal valley-fill lowstand systems tract as a continuous, one-channel-thick unit of fluvial gravel and coarse sand in the incised valley (Allen and Posamentier, 1993). Because the incised valley in the Gironde Estuary was a zone of sediment trapping during transgression, the bulk of the valley fill lies in the transgressive systems tract, consisting of landward-thinning tidal-estuarine sand and mud, estuary-mouth sands, and nearshore-marine sand. The upper part of the estuary fill is a highstand systems tract forming a seaward-prograding, tide-dominated estuarine bayhead delta.

Three-Dimensional Facies Architecture

The three-dimensional sandstone architecture of reservoirs in the C members is extremely heterogeneous as a result of the tide-dominated deltaic system. The sandstone architecture is dominated by a system of narrow (<2,000 ft [<610 m] wide), dip-elongate and dip-parallel, northeast-trending sandstone bodies (fig. 8). Because the strong northeast-trending grain of the sandstone bodies may result in anisotropic reservoir drainage patterns, it must be considered in the design and identification of new infill-well locations, recompletions, and waterflood programs in the LL-652 area.

In the tide-dominated deltaic facies tract, systematic changes occur in sandstone geometry and in sandstone partitioning according to type of stratigraphic succession (fig. 15). Net- and percent-sandstone patterns in the lower delta-plain facies tract are typically complex and reticulated, whereas in the distributary-channel and channel-mouth-bar facies tract they are dip elongate and bifurcating. In progradational sequences the sandiest parts of the deltaic system are the delta-front and distributary-channel–channel-mouth-bar facies, whereas the distal delta-front and lower delta-plain facies are relatively muddy (fig. 15). In retrogradational sequences the sandiest part of the deltaic system is the distributary channel–channel-mouth bar, whereas both the proximal and distal delta front are sandstone poor. Delta-front deposits in retrogradational submembers typically contain only 20 to 30 percent sandstone, in contrast to the relatively sandstone-rich distributary-channel system. In aggradational sequences where deposition was sufficient to keep pace with rising sea level, the dominantly preserved facies are distributary channel, channel-mouth bar, and proximal delta front, the distributary-channel facies being sandier than the delta-front facies. Relative sandiness varies little in the interdistributary–tidal-flat facies (lower delta plain) between progradational and retrogradational cycles in the LL-652 area. This part of the deltaic facies tract was an area of sediment bypass in progradational cycles, when coarse sediment was stored in the delta-front and channel-mouth-bar facies. During retrogradation, relatively more sediment was stored in the distributary channels than in the delta front, but interdistributary areas were relatively muddy. The lower delta-plain facies tract in retrogradational sequences is therefore inferred to contain multiple sites of permeability contrasts that may represent numerous but small stratigraphic traps for remaining mobile oil. Excellent examples of genetic depositional episodes (submembers) that have high-reservoir-quality sandstone encased in muddy interdistributary deposits are the Upper C-4-X and Middle C-3-X submembers. Although these two submembers together account for most of the production in the combined C-3-X–C-4-X members (fig. 3), they still contain a high potential for secondary oil production.

In the volumetrically significant facies, the dominant sandstone-body trends and shapes are ribbons and belts, whereas in other facies the sandstone bodies occur as sheets having no dominant trend. Facies that have moderate internal heterogeneities—delta front, distributary channel, tidal channel, and fluvial-estuarine channel—differ slightly in where these internal heterogeneities occur. For example, in the delta-front facies, maximum reservoir-quality sandstone is at the top of the upward-coarsening section, where silt and mud were winnowed out by wave and tidal processes. Distributary-, tidal-, and fluvial-estuarine-channel facies are expected to contain the best reservoir-quality sandstone toward the base (for example, fig. 14), where the grain size of the sandstone is maximum. However, the lower part of the channel facies also commonly contains clay clasts; organic fragments; and intraformational channel-margin, bank-collapse material that limit reservoir quality. The distal delta-front facies, although volumetrically significant, contain numerous internal heterogeneities (multiple shale interbeds) that limit vertical reservoir communication. The remaining facies (transgressive sand shoal, shelf, and tidal flat) are internally heterogeneous or muddy and may be difficult to develop efficiently.

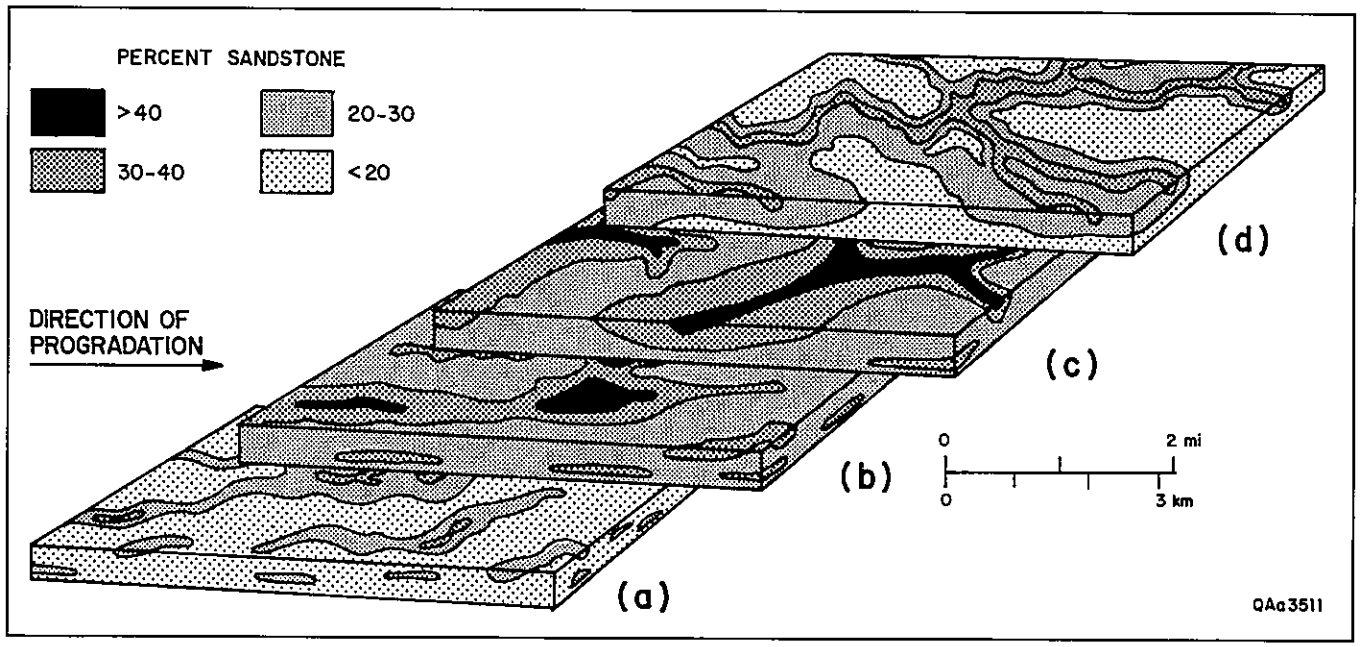


Figure 15. Typical percent-sandstone patterns in offlapping, progradational sequences in the tide-dominated deltaic facies tract, C members, LL-652 area, showing superposition and basinward progradation of (a) distal delta-front, (b) proximal delta-front, (c) distributary-channel and channel-mouth-bar, overlain by (d) lower delta-plain facies. The sandiest part of the facies tract is the distributary channel and channel-mouth bar.

Permeability Trends and Diagenetic Controls on Reservoir Quality

Reservoir Diagenesis

Depositional environment determines distribution of permeable reservoir sandstones in the C members, separated by low-permeability mudstones. Diagenesis has, however, significantly altered reservoir characteristics through compaction and cementation. Volume of quartz cement, in particular, influences reservoir quality, and because the volume of quartz cement increases significantly with depth, reservoir quality decreases with depth.

Framework Mineralogy

Framework-grain composition of C-member sandstones varies among facies (fig. 16a), the most quartz-rich samples occurring in the fluvial-estuarine-channel facies in the Lower C-6-X submember. Whereas transgressive sand-shoal, distal delta-front, and delta-front facies have intermediate framework-grain compositions, distributary-channel and tidal-channel facies contain the greatest volume of rock fragments (fig. 16a). Delta-front and transgressive sand-shoal sandstones probably contain a higher percentage of detrital quartz because wave and current abrasion disaggregated more of the mechanically unstable rock fragments and because differences in hydraulic properties allowed wave and current action to winnow quartz from rock fragments. Distributary- and tidal-channel sandstones contain more abundant rock fragments because they were not winnowed. The high percentage of quartz in the fluvial-estuarine-channel deposits cannot be explained by depositional processes, and it is likely that these incised channels tapped a different, more quartz-rich source area.

Lower Eocene sandstones are sublitharenites (fig. 16b), the average composition being $Q_{82}F_6R_{12}$. C-3-X, C-4-X, and C-6-X sandstones are slightly more

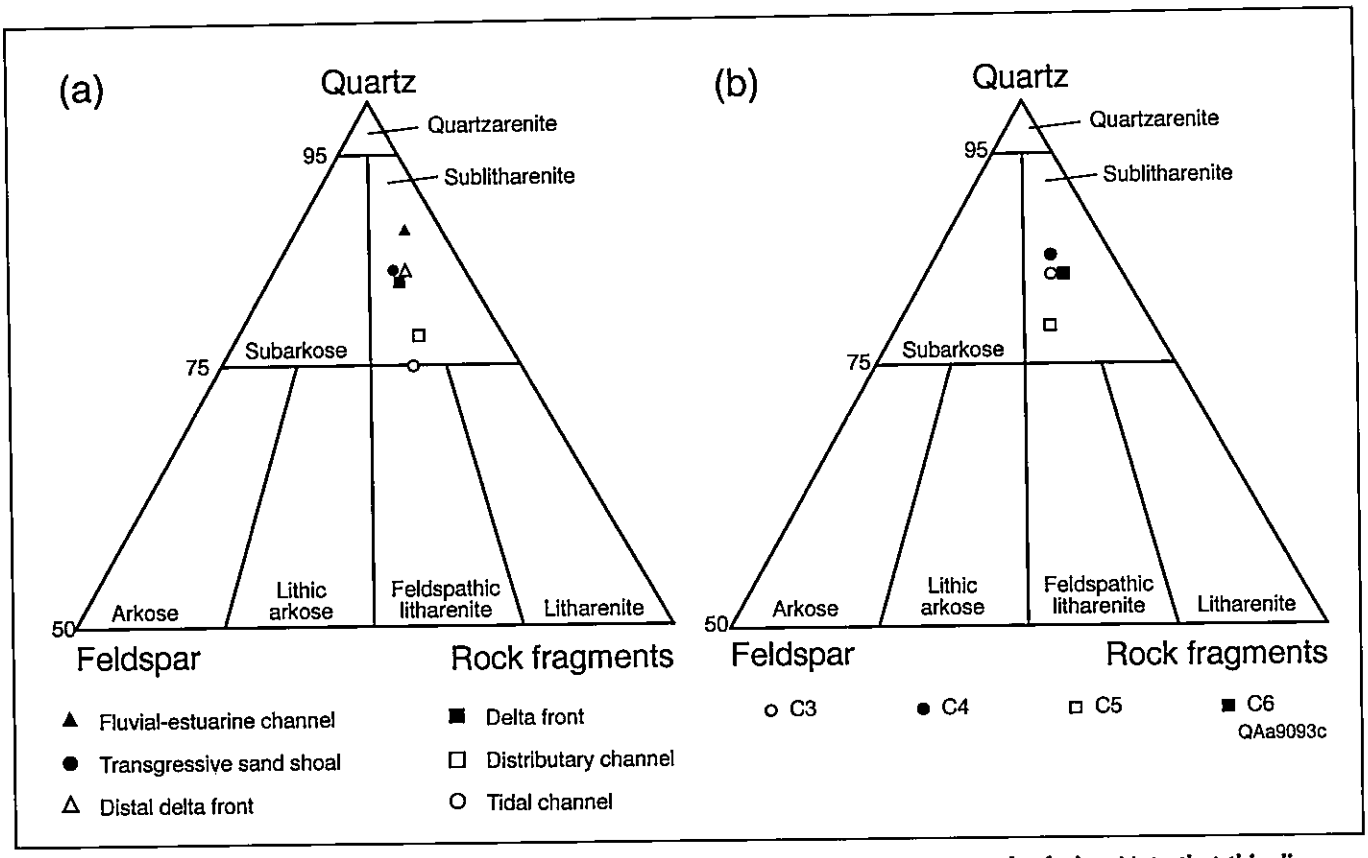


Figure 16. (a) Average compositional classification of lower Eocene sandstones, LL-652 area, by facies. Note that this diagram shows only the upper one-half of the Folk (1980) sandstone classification triangle, from 50 to 100 percent quartz. (b) Average compositional classification by member, showing only minor differences.

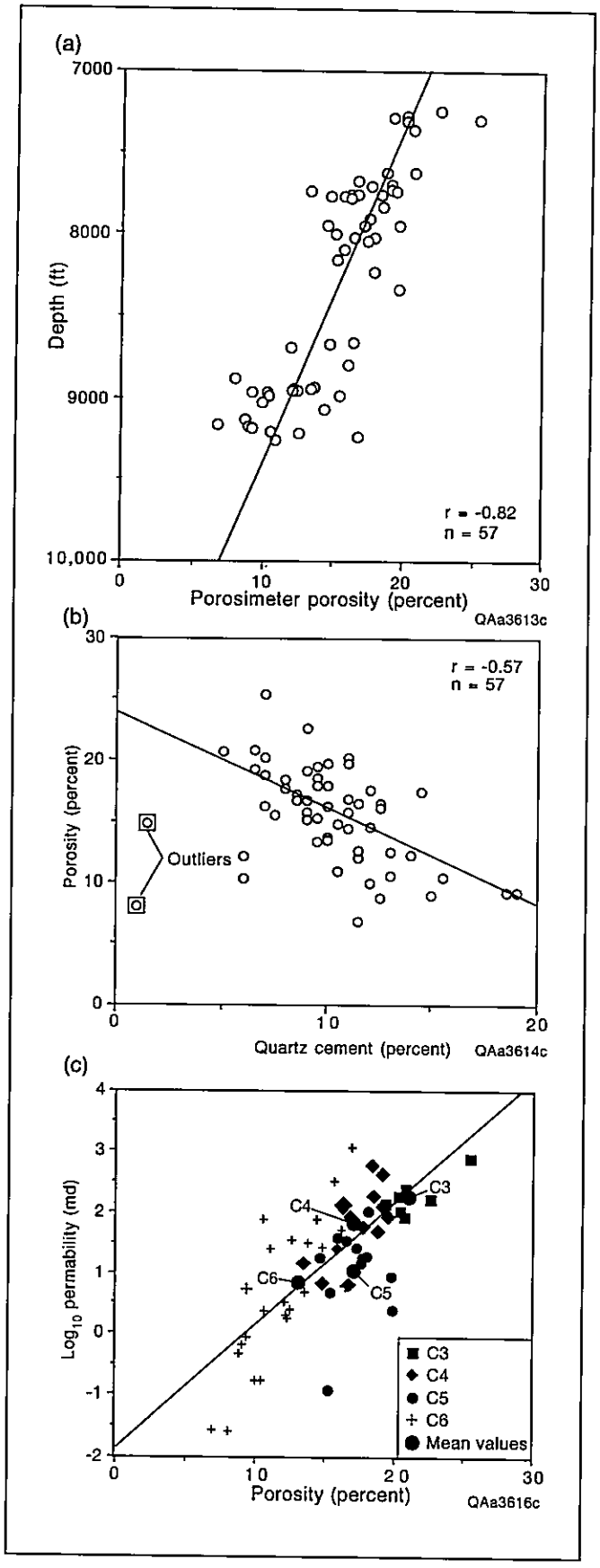
quartz rich than are C-5-X sandstones. Detrital quartz, composing an average of 58 percent of the total rock volume, forms between 61 and 97 percent of the primary constituents. Plagioclase, the most abundant type of feldspar, has an average volume of 3.5 percent; orthoclase, which is rare, has an average volume of only 0.04 percent. Because some feldspar was dissolved during diagenesis, the volume is now occupied by secondary pores or secondary pores filled by kaolinite or calcite cement. If we assume that all the open secondary pores and all the secondary pores filled by calcite or kaolinite were originally feldspar grains, the original detrital sandstone was probably a subarkose having a $Q_{76}F_{13}R_{11}$ composition.

Diagenetic Controls on Reservoir Quality

Depth and volume of quartz cement are the major controls on porosity in lower Eocene sandstones. Porosity decreases with increasing depth in the 57-sample petrographic data base, from an average of 21 percent at 7,200 ft (2,195 m) to 11 percent at 9,200 ft (2,805 m) (fig. 17a). Porosity shows the same significant decrease with depth when samples from only one facies are considered. Distributary-channel samples have an average porosity of 20 percent at 7,200 ft (2,195 m) and 10 percent at 9,200 ft (2,805 m). Differences in average porosity among facies are mainly a function of the depth from which the samples were taken.

The other parameter that correlates strongly with porosity is volume of quartz cement (fig. 17b). Because quartz-cement volume increases with depth, porosity decreases. The scatter in the relationship between quartz-cement volume and porosity (fig. 17b) indicates that quartz cement is not the only control on porosity, although it is the single most important petrographic factor. The decrease in porosity with depth is thus explained mainly by the increase of quartz cement with depth.

Porosity is the best predictor of permeability (fig. 17c), and there is a good linear trend between



porosity and log permeability when data from all sandstone intervals are combined. Both primary and secondary porosity contribute to permeability, which indicates that secondary pores are not isolated but are connected to the flow paths by primary pores. Porosity and permeability decrease systematically from the C-3-X to the C-6-X sandstones (fig. 17c).

Porosity is not an independent variable but is in turn controlled by other factors. The independent petrographic parameters that correlate significantly with permeability are volume of ductile grains, quartz cement, and authigenic illite. Ductile grains are defined in this study as metamorphic rock fragments, sedimentary rock fragments (sandstone, siltstone, and shale, but not chert), biotite, muscovite, and organic matter. All of these grains are easily deformed during burial, resulting in a loss of porosity and permeability by mechanical compaction. As the volume of ductile grains increases, therefore, permeability decreases. Quartz and illite volume also correlate significantly (at the 99-percent confidence level) with permeability. Grain size is an unimportant control on permeability in lower Eocene sandstones. Although the coarsest grains are found in C-6-X sandstone, they have low permeability because of deep burial and resulting abundant quartz cement.

Figure 17. (a) Porosimeter-measured porosity as a function of present burial depth, C-3-X through C-6-X sandstones. Porosity decreases significantly with depth. (b) Porosimeter porosity as a function of quartz cement volume, C-3-X through C-6-X sandstones. Porosity decreases significantly with increasing quartz cement. (c) Plot of log permeability versus porosity for these 57 samples. Mean values for each member are shown.

Petrophysical Evaluation

Petrophysical analysis of lower Eocene reservoirs in the LL-652 area included integrating core and log data, quantifying petrophysical properties from wireline logs, and validating petrophysical properties by comparing reservoir-volumetric maps with net-sandstone and log-facies maps. For shaly-sandstone log analysis, factors such as availability of porosity logs and core data, formation-water salinity and its variability, type and distribution of clay, shale volume (V_{sh}), and heavy minerals were determined as important parameters for selecting and developing petrophysical models for calculating porosity, permeability, and water saturation. Petrophysical models were determined by calibrating log with core data. Porosity, the key parameter required in petrophysical characterization, was derived indirectly from nonporosity logs such as gamma ray, spontaneous potential, and resistivity. The petrophysical models of the LL-652 area were developed from a total of approximately 1,500 core data points and wireline logs in 6 cored wells (fig. 4).

Model for Calculating Shale Volume (V_{sh})

The V_{sh} model was important for water-saturation and porosity calculations in the LL-652 area. The gamma-ray index of shale volume (I_{GR}) is defined as

$$I_{GR} = \frac{GR - GR_{min}}{GR_{max} - GR_{min}}, \qquad (1)$$

where GR, GR_{min}, and GR_{max} are the gamma-ray values at well log depth, clean sandstone, and shale, respectively. Whereas the linear model is $V_{sh} = I_{GR}$, the Johnson and Linke model (1978) for Tertiary deposits is nonlinear. The latter model was developed by calibrating I_{GR} with total V_{sh} values estimated from thin sections. In this study, because thin sections were taken only in clean sandstones, estimated V_{sh} values were unavailable in shaly intervals. The linear model was selected because both porosity and water saturation values derived from a linear model have a better match to core porosity, permeability, and water saturation.

Porosity Model (V_{sh}–Porosity Transforms)

In the C members, porosity generally tends to decrease because of increased quartz overgrowths with depth. To account for this depth effect, V_{sh}–porosity transforms were developed for each member. Both core-porosity and density-porosity data were used to develop V_{sh}–porosity transforms. Core porosity is biased toward clean sandstones, and density porosity is affected by borehole washouts. However, because washouts are greater in shaly intervals than in sandy intervals, good density porosity data, obtained after filtering by using caliper and porosity cutoffs, are also biased toward clean sandstones. Essentially, both core and density porosities are biased toward sandstones, and so we determined the relationships between V_{sh} and porosity initially by linear regression using the Reduced-Major-Axes (RMA) method and subsequently by adjusting the slope of the regressed lines to match foot-by-foot core porosities and permeabilities in the key wells. Because permeability is highly sensitive to the error in porosity estimation and because porosity obtained from the V_{sh}–porosity transforms depends on GR_{min} and GR_{max} values, GR_{min} and GR_{max} were adjusted slightly to approach core porosity and permeability. We found that shale porosity (microporosity) decreases with depth from 4.5 percent in the C-3-X member to 2 percent in the C-6-X member. This decrease of microporosity with depth was also documented by the petrographic study.

As shown in track 3 of figure 18a in the LL-2850 well (7,285 to 7,315 ft [2,221 to 2,230 m]) and that of figure 18b in the LL-3080 well (9,057 to 9,070 ft [2,761 to 2,765 m]), in zones of good density-log response, porosity derived from the GR log using V_{sh}–porosity transforms matches both density and core porosity within about two porosity units. In washed-out intervals (9,000 to 9,056 ft [2,744 to 2,761 m] and 9,071 to 9,200 ft [2,766 to 2,805 m], indicated by shaded areas), on the other hand, porosity derived from the GR log using V_{sh}–porosity transforms matches core porosity within two porosity units.

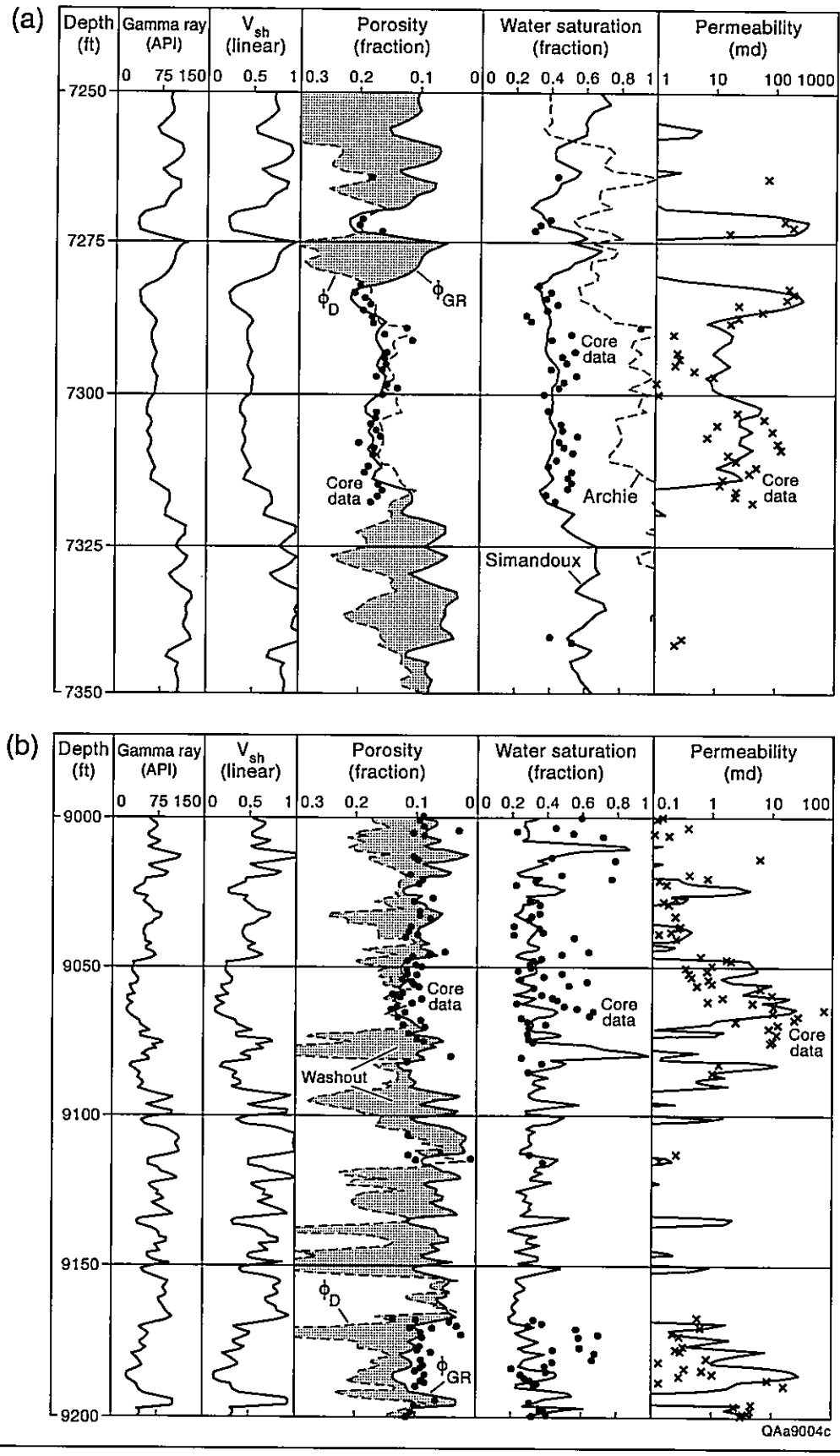


Figure 18. (a) Comparison of petrophysical properties between core data and those calculated using porosity values derived from V_{sh}–porosity transforms, C-3-X member, LL-2850 well. (b) Comparison of petrophysical properties between core data and those calculated using porosity values derived from V_{sh}–porosity transforms, C-6-X member, LL-3080 well.

Permeability Model (Permeability–Porosity Transforms)

Permeability of shaly sandstones is a function of porosity, pore type, particle size, sorting, clay type and distribution, and degree of cementation. Only porosity can be derived from conventional logs, however, and permeability is then calculated by permeability–porosity transforms obtained from core data. The ranges of scatter in permeability and porosity crossplots in lower Eocene sandstones are two to three orders of magnitude, which were caused by factors other than porosity. Researchers have expended much effort to determine the effect of each factor on permeability (Beard and Weyl, 1973; Neasham, 1977; Herron, 1987). Neasham (1977) showed that pore-bridging clays reduce permeability more effectively than pore-filling or pore-lining clays by one order of magnitude. The recently developed geochemical logs, which provide foot-by-foot information about cement and clay types, were designed to improve permeability estimates (Herron, 1987).

Average permeability values differ greatly between the C-3-X and C-4-X members and the C-5-X, C-6-X, and C-7-X members. Average permeabilities are 30 millidarcys (md) in the C-3-X and C-4-X members and only 1 md in the C-5-X, C-6-X, and C-7-X members. These differences suggest depth control on permeability, which varies greatly by member because average porosity decreases with depth.

Comparisons between permeability calculated by these transforms and core permeability (shown in track 5 in fig. 18) reveal that permeability values are consistent in most intervals. The transforms for the C-5-X, C-6-X, and C-7-X members tend to underestimate the high permeability in core data. It is because the gamma-ray curve inadequately records thin sandstones that permeability is consequently underestimated.

Water-Saturation Model

Petrophysical parameters used in log analysis (formation-water salinity [11,000 ppm], water resistivity [0.50 ohm-m], cementation exponent m [2.0], and saturation exponent n [2.0]) were used to calculate water saturation (S_w) in each key well from the Archie, Simandoux, Indonesian, and Waxman–Smit models (Asquith, 1990). As shown in track 4 in figure 18a, the Archie equation always calculates too high a water saturation, and the Simandoux model matches water saturations measured from cores well. On track 2 of figure 19a, Indonesian, Simandoux, and Waxman–Smit models are compared. The Waxman–Smit equation tends to calculate too high a water saturation, whereas the Simandoux and Indonesian equations match the correlation well. The Simandoux model relates resistivity to the total (laminated and dispersed) volume of shale by

$$S_w = \frac{0.5R_w}{\phi^2}\left(\sqrt{\frac{4\phi^2}{R_wR_t}+\left(\frac{V_{sh}}{R_{sh}}\right)^2}-\frac{V_{sh}}{R_{sh}}\right), \qquad (2)$$

where R_w, R_{sh}, and R_t are the resistivities of water, shale, and formation, respectively; ϕ is the porosity; and V_{sh} is the volume of shale.

Finally, the petrophysical model was used to evaluate C members in the six key wells. Water saturations calculated by the Simandoux equation were matched to water saturations from core (fig. 18), and data obtained from core and well logs revealed a general trend of water saturation decreasing with depth. Average water saturation is about 40 percent in the C-3-X and C-4-X members and about 30 percent in the C-5-X, C-6-X, and C-7-X members. This difference may result because the shale effect is more pronounced in the C-3-X and C-4-X members, whereas the quartz cement effect is more pronounced in the C-5-X, C-6-X, and C-7-X members. Microporosity associated with shale causes high capillary-trapped water saturation and high apparent water saturation. The water saturation in sandstone is actually much lower than the apparent water saturation, which may explain why a negligible amount of water was produced from most wells in the C-3-X and C-4-X members displaying high apparent water saturations.

At water salinity of about 11,000 parts per million (ppm), the water saturation values calculated by equation using n values of 2.00, 2.02, and 2.04 were compared with those from core at 9,000 to 9,200 ft (2,744 to 2,805 m) in the C-6-X member in the LL-3080 well. Although the n values of 2.00, 2.02, and 2.04 are within the limit of measurement error, the calculated water saturation varies by more than 20 percent in many intervals. Water saturations, calculated using n = 2.00, indicate that these intervals are highly oil saturated, whereas those calculated using n = 2.02 and n = 2.04 indicate that these intervals are wet. Because porosity values are lower than 8 percent, high water saturations are expected. The low water

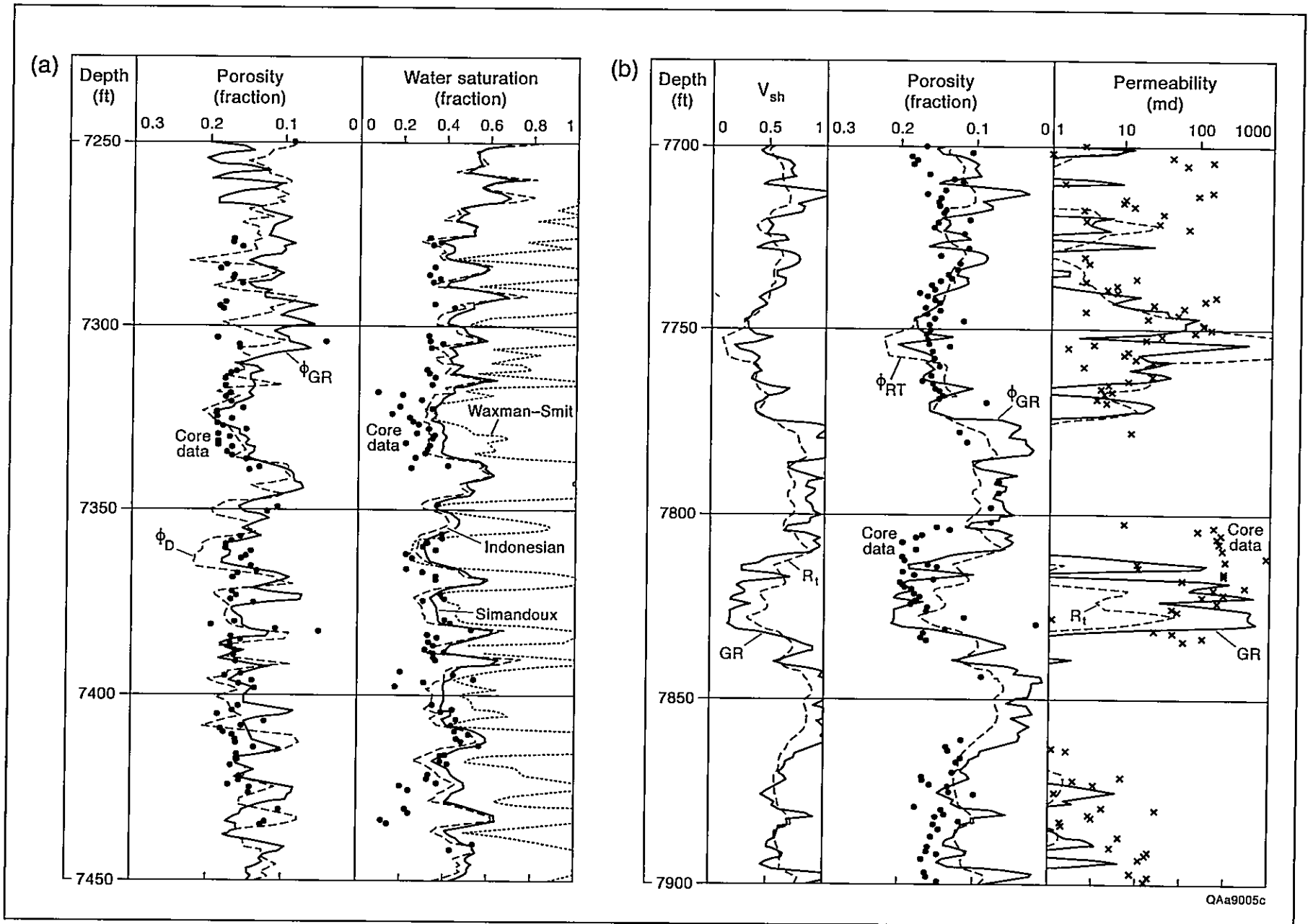


Figure 19. (a) Comparison of water-saturation values calculated by Indonesian, Simandoux, and Waxman–Smit models. (b) Comparison of V_{sh}, porosity and permeability derived from gamma-ray and resistivity logs. Data are from C-3-X member, LL-3282 well.

saturations calculated using n = 2.00 are thus most likely incorrect. This is clearly one of the drawbacks of the Simandoux equation at low salinity and porosity. This discrepancy can be eliminated, however, by careful selection of cutoff values for porosity and V_{sh}.

Cementation and Saturation Exponents

Predominant clays in the C members are kaolinite, chlorite, and illite, which have the effect of increasing conductivity and, in turn, reducing the cementation exponent (m) and saturation exponent (n). Overburden pressure also affects both cementation and saturation exponents slightly. Data from special core analyses indicate that m increases from about 1.80 without overburden pressure to 1.90 with 4,600 or 6,000 pounds per square inch (psi) overburden pressure. Similarly, n increases from about 1.48 without overburden pressure to 1.70 with 4,600 psi overburden pressure. After correcting shaliness using the Waxman–Smit equation, we adjusted both m and n, which are the values used in the well log analysis, to 2.00.

Fieldwide Formation Evaluation and Validation by Mapping

After developing petrophysical models from data from cored wells, we applied them to analyzing 65 other wells with GR logs and 39 wells without GR logs. V_{sh} was derived from SP or resistivity logs in 34 other wells without GR and density logs. The V_{sh} calculated from SP logs is given by

$$V_{sh} = \frac{SP - SP_{min}}{SP_{max} - SP_{min}}, \qquad (3)$$

where SP is log value, SP_{min} is SP of clean sandstone, and SP_{max} is SP of shale. Base-line shifting and selecting clean sandstone values were the major problems in using SP logs to calculate V_{sh}. Calculations were done by section whenever the base line shifted. If SP logs could not be used, resistivity logs were used to estimate V_{sh} as

$$V_{sh} = \left(\frac{R_{sh}}{R_t}\right)\left(\frac{R_{max} - R_t}{R_{max} - R_{sh}}\right)^{\frac{1}{b}}, \qquad (4)$$

where R_{sh} is resistivity of adjacent shale, R_t is the measured resistivity, R_{max} is the maximum resistivity of the clean pay zone, and b is an empirical exponent (Terra Science, 1993). The uncertainties about V_{sh} calculated by resistivity were greater than those about V_{sh} calculated by GR or SP. R_{max} and b were selected by trial and error, and V_{sh} is sensitive to the value of the b exponent, which ranged from 2.0 to 3.5 and normally increased with the mean porosity of each member. When this method is used and b values are carefully selected, the porosity calculated from resistivity logs agrees well with those calculated from density and GR logs (fig. 19b).

Net-Pay Determinations

We determined net-pay-thickness values using cutoff values of V_{sh}, water saturation, and porosity. Only the V_{sh} cutoff values were used for calculating net sandstone thickness. The relationship of V_{sh} to net sandstone thickness in each member was determined from net sandstone thickness counted from cores. S_w cutoff was determined from resistivity logs. For the C-1-X to C-4-X members, the resistivity cutoff was determined to be 10 ohm-m; for the C-5-X member, 12 ohm-m; and for the C-6-X member, 14 ohm-m. Although porosity and permeability are too low for the C-7-X member to be productive, this interval is still considered prospective in sandstones having resistivity greater than 25 ohm-m and porosity greater than 8 percent.

Production data were also used to validate results of petrophysical evaluation and cutoff values. Twelve production logs were used from the LL-1001, LL-1156, LL-1876, LL-2010, LL-2089, LL-2187, LL-2938, LL-3062, LL-3074, LL-3075, LL-3155, and LL-3156 wells (fig. 4). Open intervals having less than 8 percent porosity and more than 55 percent water saturation were considered nonproductive. Cutoff values of S_w for net sandstone and net pay thicknesses were further modified during mapping. They were determined to be 55 percent for the C-1-X to C-4-X members and 50 percent for the C-5-X to C-7-X members. The higher cutoff in water saturation for the C-3-X and C-4-X members reflected a shale effect that is more pronounced in the C-3-X and C-4-X members and a cement effect that is more pronounced in the C-5-X, C-6-X, and C-7-X members.

Sandstone Architecture and Recovery Optimization of Reservoir Intervals

Depositional Controls on Net Pay and SoPhiH

Net-oil-sandstone (net-pay) and SoPhiH maps of the C members and submembers exhibit northeast-trending patterns, reflecting depositional control on reservoir geometry (compare figs. 21 through 25). Net-pay contours extend across the field in most members and submembers, although in some intervals net pay thickness decreases northeastward, reflecting seaward (northeastward) pinch-out of delta-front sandstones. Structural influences are indicated by abrupt changes in net-pay values across faults, particularly in the southwest and northeast parts of the field. Net-pay contours on the south and southeast limbs of the field are closely spaced and result from oil–water contacts.

Reservoir Examples

Two submembers (Upper C-4-X and Middle C-3-X), important reservoir intervals in the C-4-X and C-3-X members, together account for 82 percent of the lower Eocene oil production in the LL-652 area (fig. 3), although these submembers represent different depositional sequences. The Upper C-4-X submember contains multiple progradational wedges in an overall backstepping, retrogradational sequence, and the Middle C-3-X submember represents a brief but major period of extreme deltaic offlap (fig. 2b).

Upper C-4-X Submember

The Upper C-4-X submember consists of strata from the no. 14 shale marker to the top of the C-4-X member (fig. 3). The Upper C-4-X submember is composed of four main, dominantly upward coarsening units as part of the major backstepping, retrogradational cycle that makes up the Upper C-4-X submember (fig. 20).

Sandstone-Body Geometry, Lithology, and Depositional Systems

The Upper C-4-X submember is composed of northeast-trending, dip-elongate sandstone bodies that have a combined thickness of 90 to 140 ft (27.4 to 42.7 m), separated by sandstone-poor areas containing less than 50 ft (<15.2 m) of net sandstone (fig. 21). Thickest net-sandstone trends (>100 ft [>30.5 m]) occur as four belts in the LL-652 area.

Unit no. 4, representing proximal delta-front and lower delta-plain deposits in an initial advance of a delta in the LL-652 area, contains a distributary-channel complex in the LL-2850 core (fig. 20). Deltaic progradation was from the southwest to the northeast, and individual units in the Upper C-4-X submember thicken slightly northeastward, reflecting basinward subsidence. Delta-front sandstones of unit nos. 1, 2, and 3 are progressively shalier northwestward because of increasing amounts of thin mudstone interbeds. Unit no. 1 represents retrogradational deposits associated with the laterally extensive marine flooding surface at the top of the Upper C-4-X submember (fig. 20).

Porosity and SoPhiH

The Upper C-4-X submember contains the highest arithmetic average porosity in the southwest and northwest parts of the field (fig. 22a). The great variability and spatial complexity in porosity in the Upper C-4-X submember impart a high degree of heterogeneity to this submember, making it an excellent candidate for infield development. Remaining oil may be stratigraphically trapped in isolated, high-porosity (>18 percent) areas in the central part of the field and may also be structurally trapped in the north-northeast-trending zone of reverse faults.

SoPhiH reaches a maximum of 26.6 ft (8.1 m) in the Upper C-4-X submember (fig. 22b). High SoPhiH values primarily reflect thick net-pay values (fig. 22c). Greatest SoPhiH values (>10 ft [>3 m]) correspond to

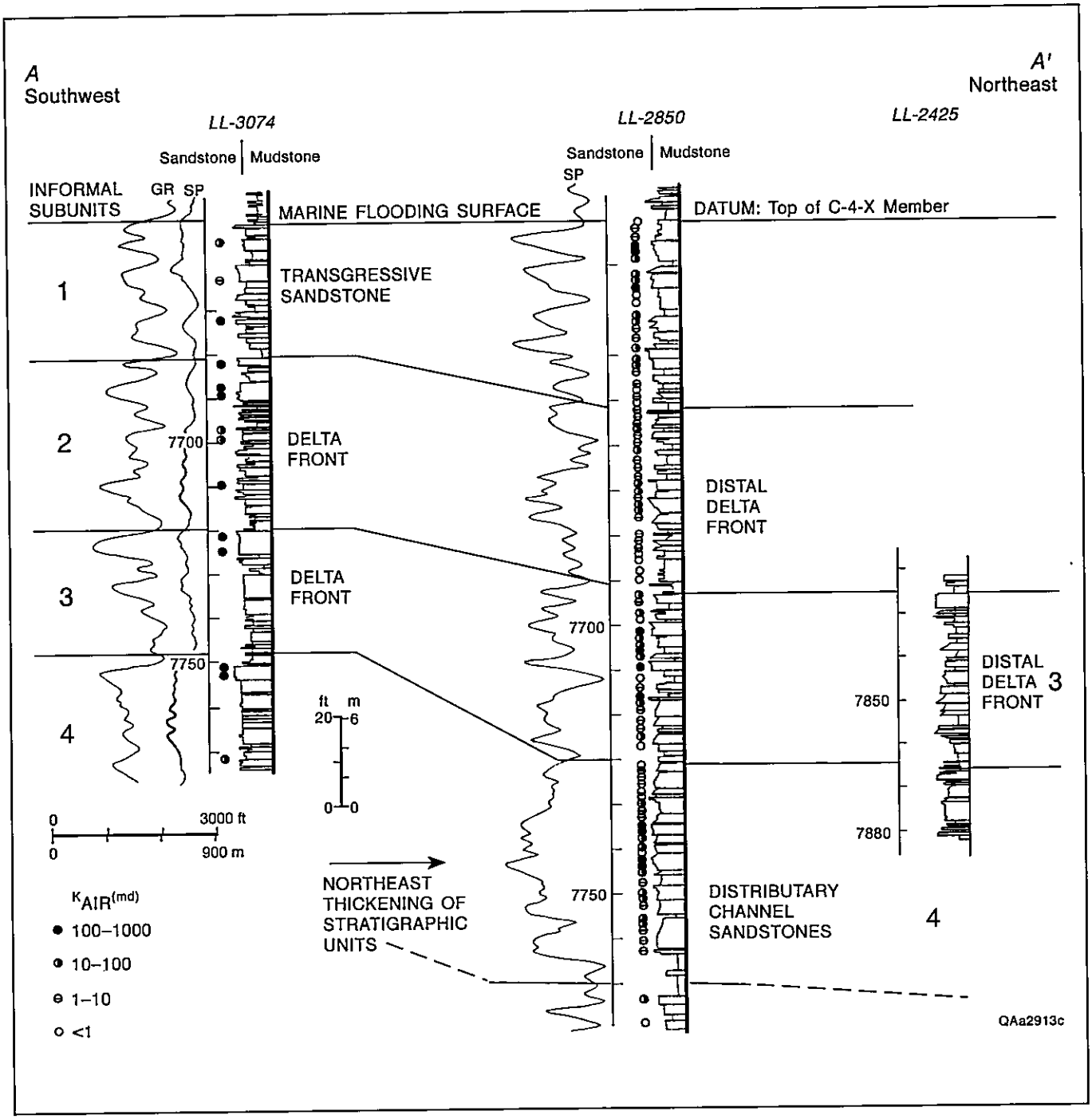


Figure 20. Southwest-northeast stratigraphic dip cross section A–A′ from cores, Upper C-4-X submember, showing permeability variation and basinward thickening of subunit nos. 1 through 4 in the transition from proximal to distal delta-front facies. Line of section shown in figure 21.

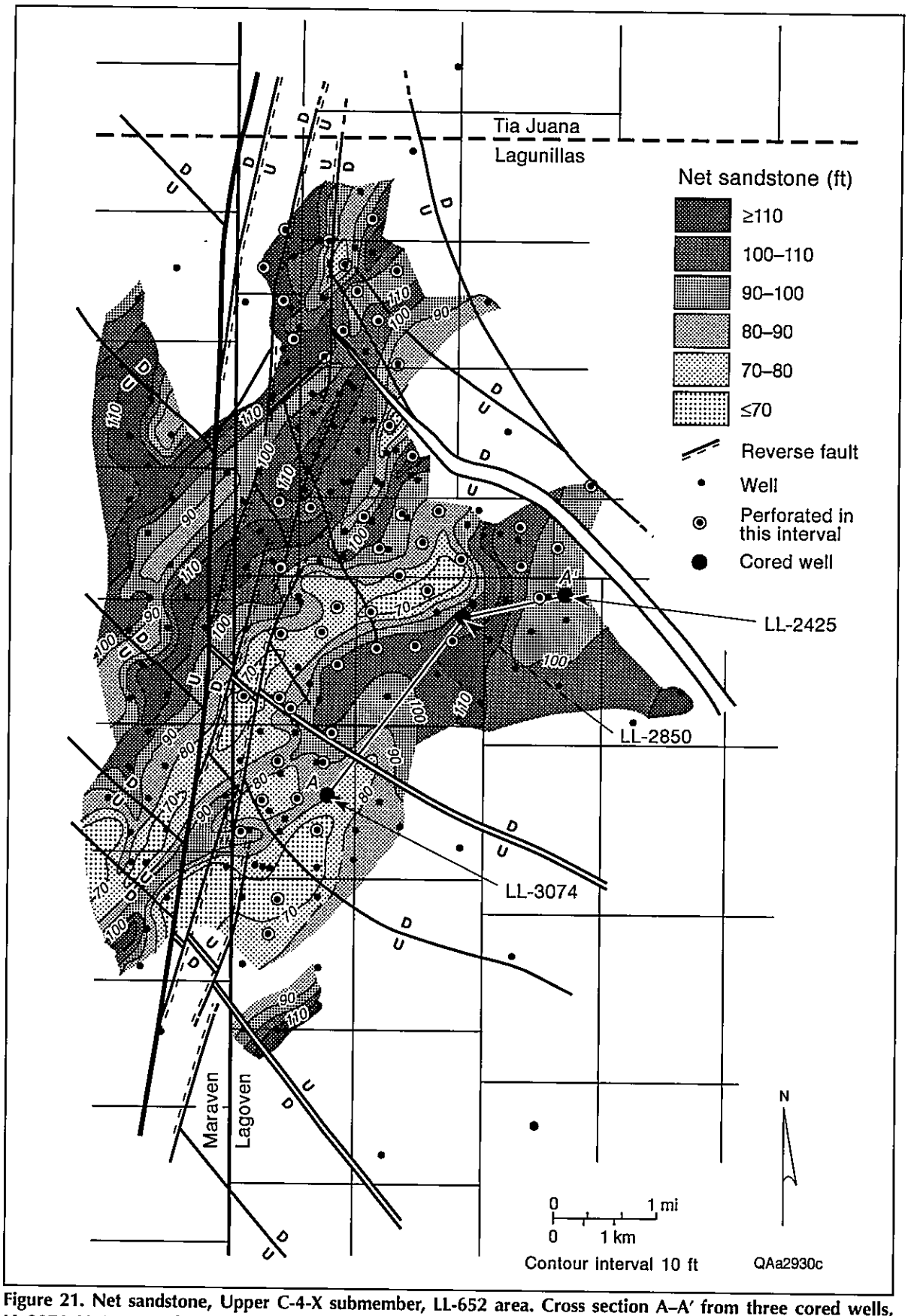


Figure 21. Net sandstone, Upper C-4-X submember, LL-652 area. Cross section A–A′ from three cored wells, LL-3074, LL-2850, and LL-2425, shown in figure 20.

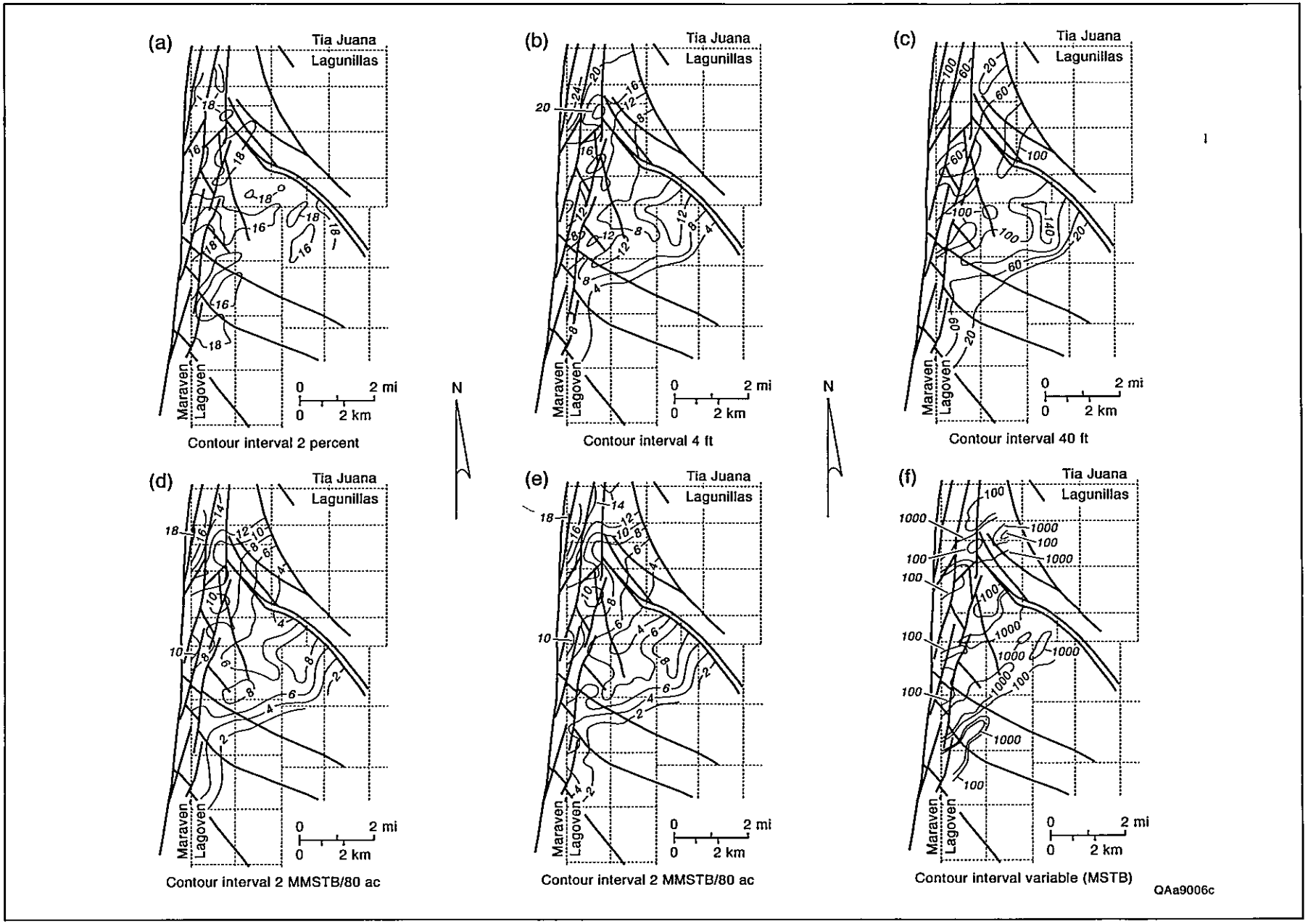


Figure 22. Maps of reservoir volumetrics, Upper C-4-X submember, LL-652 area, including (a) arithmetic average porosity, (b) SoPhiH, (c) net pay, (d) OOIP, (e) remaining oil, and (f) cumulative oil production. Northeast-trending patterns are controlled by depositional fabric of distributary-channel and proximal delta-front deposits.

thick depositional axes of more than 100 ft (>30.5 m) of net sandstone (fig. 21), particularly in the west-central and north-central parts of the field (fig. 22b).

Net Pay, OOIP, and Remaining Oil

The Upper C-4-X submember contains the greatest pay of the three submembers in the C-4-X member, with as much as 140 ft (42.7 m) of net pay in the north part of the field (fig. 22c). Good correspondence exists between net pay thickness and net sandstone thickness in the Upper C-4-X submember (fig. 21), indicating a strong depositional control on reservoir geometry. High net pay thickness in the north part of the field is, however, partly controlled by steeply dipping strata in a structurally complex area.

The Upper C-4-X submember contains high volumes of OOIP (commonly >6 MMSTB per 80 acres in the central part of the field and >10 MMSTB per 80 acres in the north part of the field [fig. 22d]). Thick pods of more than 7 MMSTB per 80 acres of OOIP approximately correspond to thick (>80 ft [>24.4 m]) distributary-channel and proximal delta-front sandstones (fig. 21) in the central part of the field (fig. 22d). The north areas commonly contain more than 10 MMSTB per 80 acres of OOIP, coinciding with dipping strata in a northern deltaic depocenter of more than 100 ft (>30.5 m) of net sandstone thickness (fig. 21).

The Upper C-4-X submember (fig. 22e) contains more remaining oil than does the rest of the C-4-X member. Many areas, particularly in the north part of the field, contain nearly as much remaining oil as OOIP (compare fig. 22d), indicating that the Upper C-4-X submember has a high potential for secondary oil recovery. Other areas that have great volumes of remaining oil are in the central part of the field (>8 MMSTB per 80 acres) that coincide with thick (>80 ft [>24.4 m]) delta-front and distributary-channel sandstones (fig. 21).

Reservoir Development

The mature Upper C-4-X submember has been perforated extensively throughout the LL-652 area (fig. 21) and is currently undergoing rapid pressure depletion. The Upper C-4-X submember is the most productive interval in the C members, having produced from 25 wells, 14 of which have produced more than 1.5 MMSTB (fig. 22f). Despite high production in the Upper C-4-X submember, the LL-652 area has numerous sites where high volumes of remaining oil coincide with little or no production. For example, high values of remaining oil (>10 MMSTB per 80 acres) (fig. 22e) are found in the north part of the center of the field, an area of no previous production. In addition, the extreme north part of the field, where no production has occurred, is projected to have high values of remaining oil. Areas of more than 7 MMSTB of remaining oil are also in the west-central part of the field, which coincides with limited production (fig. 22f). High values of net pay (>80 ft [>24.4 m]) (fig. 22c) are found in the extreme north, nonproduced part of the field.

A final consideration in infield development of the Upper C-4-X submember is locating infill wells in the northeast-trending zone of reverse faults. Some wells in this fault zone (LL-852, LL-946, LL-1001, and LL-1196 [located in fig. 4]) have each produced more than 1 MMSTB. Numerous segments of other reverse faults in the Upper C-4-X submember, however, have not been contacted, particularly in the west part of the LL-652 area.

Middle C-3-X Submember

Sandstone-Body Geometry, Lithology, and Depositional Systems

The Middle C-3-X submember is a 70- to 100-ft (21.3- to 30.5-m) sandstone-rich interval (fig. 3) that has a sandstone geometry of dip-parallel, northeast-trending bands, 1,500 to 3,500 ft (457 to 1,067 m) wide and more than 50 ft (>15.2 m) thick (fig. 23). The Middle C-3-X submember, cored in the LL-2425, LL-2850, and LL-3074 wells, contains a lower upward-coarsening section of delta-front deposits, 14 to 20 ft (4.3 to 6.1 m) thick, commonly truncated by 8- to 14-ft (2.4- to 4.3-m) upward-fining, distributary-channel sandstones (fig. 24a). The upper part of the section contains a variety of different types of sandstone bodies, including upward-coarsening, interbedded overbank deposits (LL-3074 well); very fine and fine, ripple cross-stratified sandstones having no grain-size trends (LL-2425 and LL-2850 wells); and erosion-based, upward-fining tidal-channel sandstones (LL-2850 well). The Middle C-3-X submember is bounded above by a 10-ft (3-m) laterally continuous, mainly upward coarsening zone of irregularly calcite-cemented, transgressive sand-shoal deposits

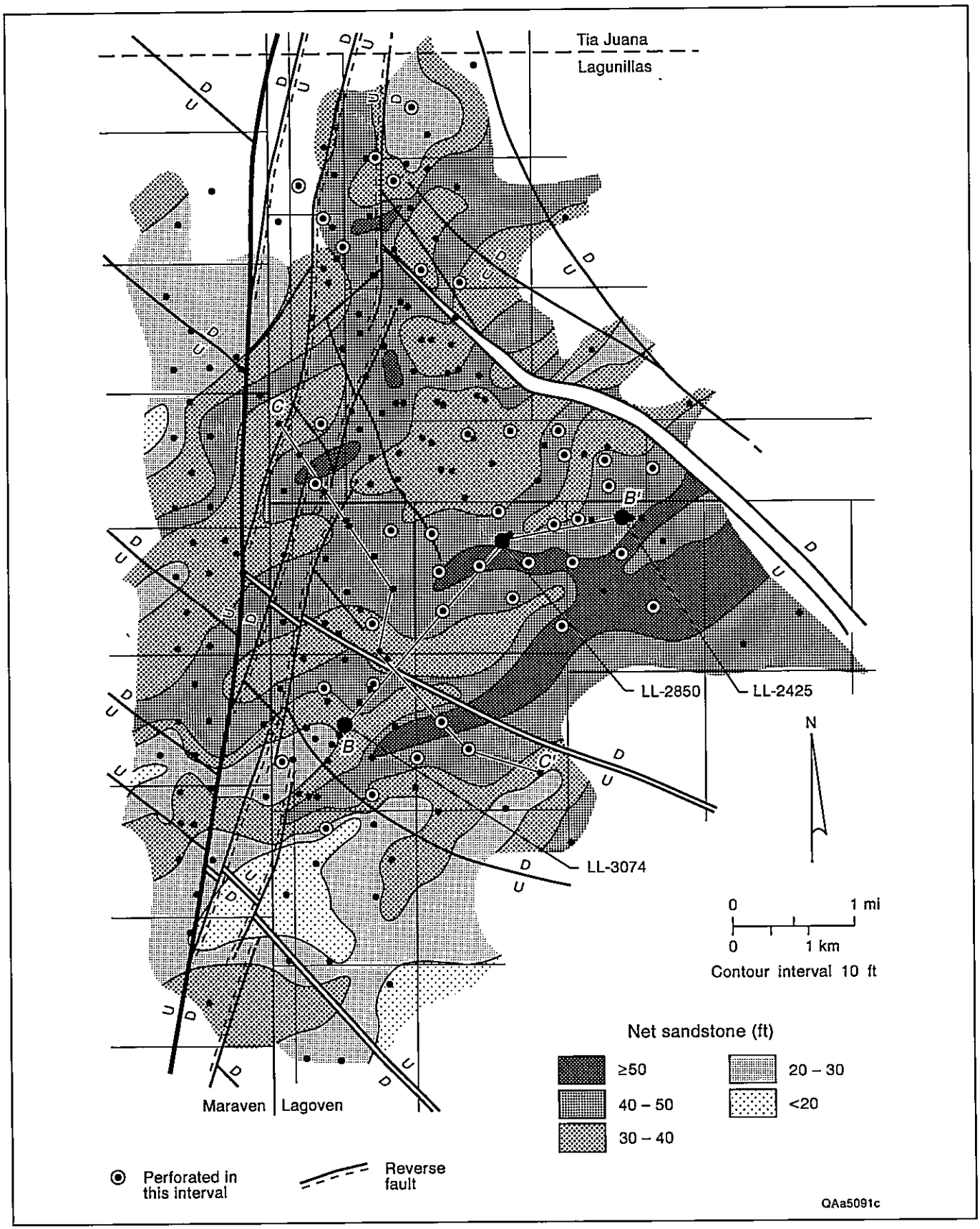


Figure 23. Net-sandstone-thickness map, Middle C-3-X submember. Dip-elongate delta-front deposits are transected in the south part of the field by a system of distributary-channel deposits more than 40 ft (>12 m) thick. Stratigraphic dip cross section B–B′ from cored wells LL-3074, LL-2850, and LL-2425 shown in figure 24a. Stratigraphic strike cross section C–C′ shown in figure 24b.

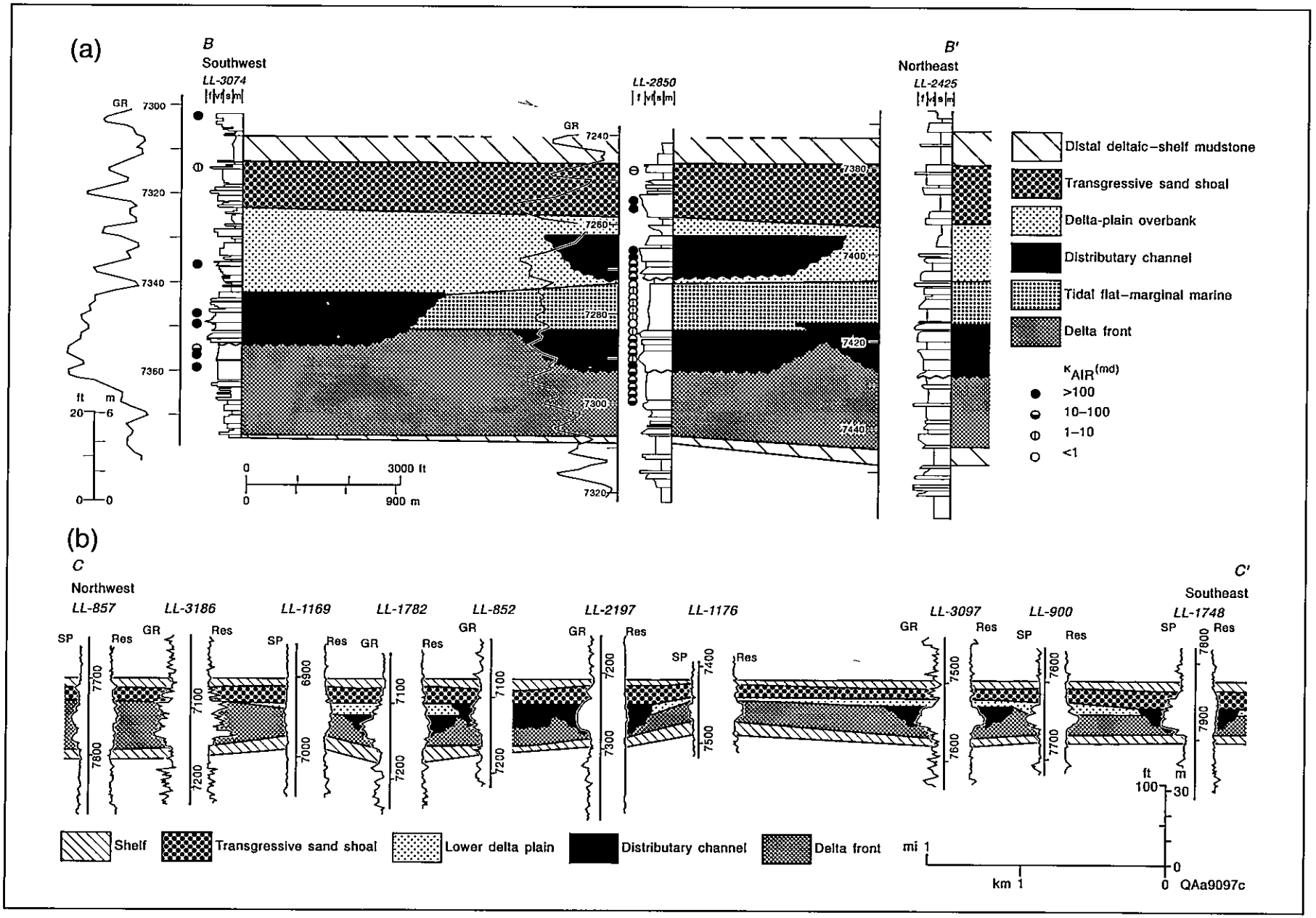


Figure 24. (a) Southwest-northeast stratigraphic dip section B–B′ from cores, Middle C-3-X submember, showing distributary-channel deposits that truncate delta-front deposits and high permeability contrast between tidal-flat and distributary-channel deposits. (b) Northwest-southeast stratigraphic strike cross section C–C′, Middle C-3-X submember, showing sandstone-body architecture and facies heterogeneity resulting from multiple lenticular, distributary-channel sandstones locally truncating muddy delta-front sandstones. The top reservoir seal is partly provided by a sheetlike, calcareous, transgressive sand-shoal deposit. Lines of sections shown in figure 23.

that are in turn overlain by a 4- to 6-ft (1.2- to 1.8-m) laterally continuous, burrowed mudstone representing a marine flooding surface.

A stratigraphic strike section that cuts across the orientation of the sandstone bodies in the Middle C-3-X submember shows lenticular distributary-channel sandstone bodies, individually about 2,000 ft (~610 m) wide, locally truncating an extensive system of delta-front sandstones (fig. 24b). These distributary-channel sandstones are bounded laterally by muddy lower delta-plain deposits that have an irregular sheet geometry. The Middle C-3-X submember is bounded below by a laterally extensive shelf mudstone and above by an irregular, transgressive sand sheet and associated shelf mudstone. Areas where high permeability and porosity contrasts occur are along (1) distributary-channel–delta-front contacts, particularly at the base of channel deposits where clay clasts and organic fragments may compose flow barriers and (2) lateral pinch-outs of distributary-channel sandstones into tidal-flat mudstones. Other flow barriers may exist in the transgressive sand-shoal–sheet facies between numerous thin and impermeable, calcite-cemented zones. These zones, however, are not easily identified from electric logs, and their lateral continuity is difficult to predict.

Porosity and SoPhiH

In the Middle C-3-X submember, arithmetic average porosity is as much as 20 percent (fig. 25a). Relatively wide belts of high porosity related to thick (>40 ft [>12 m]) distributary-channel and delta-front sandstones extend northeastward across the LL-652 area. Greatest SoPhiH values are widely distributed across the field (fig. 25b), reflecting sandstone-rich, distributary-channel, and proximal delta-front sandstones (fig. 23).

Net Pay

Net pay is distributed in multiple bands of more than 40 ft (>12 m) (but varying in width) that extend mostly across the field (fig. 25c). Most of the thicker net-pay bands correspond to depositional axes of more than 50 ft of net sandstone (fig. 23), although the band of thick net pay in the central part of the field is slightly north of the corresponding zone of more than 50 ft of net sandstone. Multiple infill targets exist in the Middle C-3-X submember because this interval is sandstone rich and internally heterogeneous. The resulting net-pay contrast ranges from 20 to 60 ft (6 to 18 m) (fig. 25c).

OOIP and Remaining Oil

Greatest values of OOIP in the Middle C-3-X submember are found in the north and east-central parts of the field (fig. 25d). These high values of OOIP in the east-central part of the field correspond approximately to thick (>50 ft [>15.2 m]) distributary-channel sandstones (fig. 23). High volumes of remaining oil lie in the east-central part of the field (>4 MMSTB per 80 acres) and in the north part of the field (>3 MMSTB per 80 acres) (fig. 25e). Volumes of remaining oil resemble those of the OOIP (fig. 25d), indicating that this submember has an excellent potential for secondary oil recovery.

Reservoir Development

Although the Middle C-3-X submember has been perforated throughout the LL-652 area (fig. 23), it continues to be an active producer, its pressure decline being less severe than that of the Upper C-4-X submember. Undrained or partly drained compartments may thus exist in this unit, and recompletions, infill wells, or even strategically implemented waterfloods may be necessary to produce the remaining mobile oil most efficiently. Areas in the field where this oil could be targeted by recompletions and infill wells are defined by structurally and stratigraphically complex areas far from previously existing completions. A limited waterflood may be appropriate in the central, unfaulted part of the LL-652 area that has been extensively perforated, where it may be able to sweep mobile oil that remains along facies contacts between distributary-channel and delta-front facies or tidal-channel and tidal-flat facies.

The Middle C-3-X submember has produced oil from 60 wells (fig. 25f). Seventeen of these wells have each produced more than 500,000 STB, most of which comes from southern and central areas, with limited production in the north. Although the Middle C-3-X submember is sandstone rich throughout the entire LL-652 area (fig. 23), broad areas have no production in the west, extreme north, and north-central parts of the field (fig. 25f). Each of these three unexploited areas contains large volumes (typically

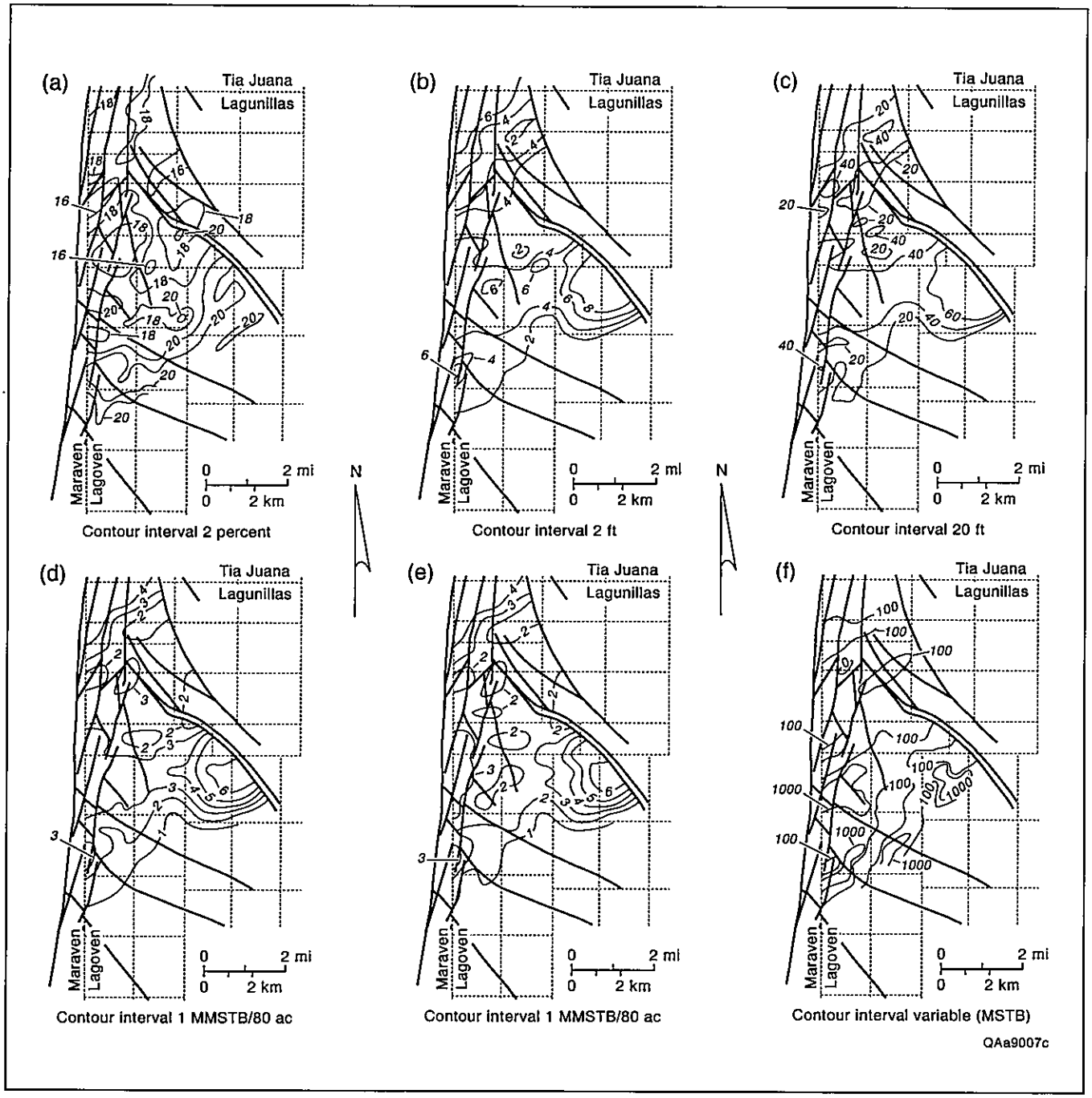


Figure 25. Maps of reservoir volumetrics, Middle C-3-X submember, LL-652 area, including (a) arithmetic average porosity, (b) SoPhiH, (c) net pay, (d) OOIP, (e) remaining oil, and (f) cumulative oil production. High volumes of remaining oil in the north part of the field are partly controlled by apparent reservoir thickening resulting from steeply dipping strata.

3 MMSTB per 80 acres) of remaining oil (fig. 25e). In addition, the east-central part of the field still contains large volumes of remaining oil (>3 MMSTB per 80 acres) (fig. 25e) in distributary-channel and proximal delta-front sandstones (fig. 23), despite the presence of six wells, each totaling more than 500,000 STB of cumulative production (fig. 25f).

The Middle C-3-X submember has also been poorly developed along the north-northeast-trending zone of reverse faults (fig. 25f). Several opportunities exist for infill wells or recompletion in this fault zone, especially in areas of high volumes of remaining oil. Examples include the west-central and north-central parts of the field (fig. 25e and 25f).

Opportunities and Strategies for Recovery Optimization and Reserve Growth

The potential for oil-field reserve additions is a function of oil volumes originally in place, level of development of the reservoir and, most important, the degree of internal geologic complexity of the field. As a result of the high degree of depositional and structural variability, reservoirs in the C members in LL-652 area exhibit considerable variation in reservoir quality and, hence, relatively low recovery efficiency. This poor recovery efficiency is a function of the weak solution-gas-drive mechanism and well spacing that is greater than the size of the reservoir compartments that collectively compose the main reservoir sandstones.

Detailed well-log correlations indicate that considerable between-well variability is also responsible for the low recovery efficiency of the LL-652 area. Wells from the same reservoir yield widely varying amounts of oil, further demonstrating even smaller scale heterogeneity. These reservoirs have a current well spacing of 80 acres and a primary recovery efficiency of 20 percent (468 MMSTB). The 923 MMSTB of unrecovered mobile oil (fig. 26) composes a major target for reserve additions and increased production.

Reservoir-rock-quality analysis focused on petrophysical and diagenetic factors (for example, pore scale distribution and clay mineralogy) that currently influence oil production and that could be critical in future advanced oil-recovery projects. Together with stratigraphic and structural complexity, rock-property variation emphasizes the fact that targeted strategies must be defined for increasing ultimate recovery. Maps of SoPhiH and remaining oil were indispensable in planning strategies for additional recovery and reserve growth. We interpreted these maps to help us plan optimal new-well locations, continued conventional development, targeted off-pattern infill drilling, well-recompletion programs, and a pilot waterflood.

Cumulative production varies greatly across the LL-652 area. Reasons for this variability include (1) age differences of producing well—old wells have had time to produce larger quantities of oil than

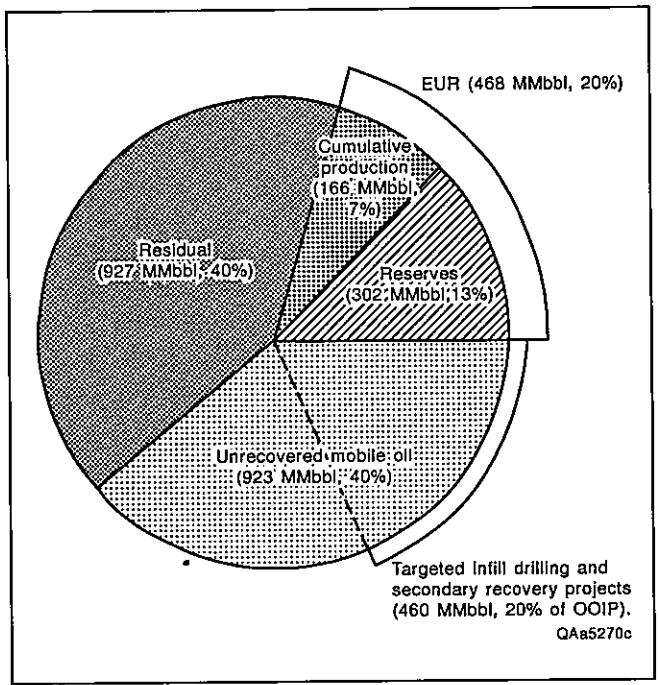


Figure 26. Reservoir volumetrics, C members, LL-652 area. An enormous resource of unrecovered mobile oil (923 MMSTB, or 40 percent of OOIP) exists in poorly drained reservoir compartments that can be contacted by strategically targeted infill wells and secondary-recovery projects such as waterflooding.

young wells, (2) greater-than-average production in areas of repeat section and enhanced fracture permeability in zones of reverse faults, (3) greater-than-average production in areas of thick net pay and net sandstone along deltaic depositional axes, and (4) differences in net thickness of intervals perforated in each submember.

We determined general areas of opportunity for optimizing oil recovery by comparing maps of cumulative production with maps of SoPhiH and remaining oil. Numerous areas exist for infill wells, particularly in the sparsely developed north part of the LL-652 area. Although these areas have little or no cumulative production, they are inferred to contain large volumes of OOIP and remaining oil. Never-

theless, the maps of remaining oil in the LL-652 area represent integration of geological, petrophysical, and production studies and show that most oil remains in areas that have high cumulative productions. These areas have the highest kh and the greatest OOIP as well. Infill-drilling and recompletion strategies were thus based on a comparison of the mutual occurrence of remaining resources, kh values, and current production.

New Extended-Development Locations

Location of new development wells was primarily directed at recovering proved hydrocarbon resources that could not be recovered by existing wells. In some cases, development wells were proposed as alternate wells or as wells to accelerate production. In the C-3-X and C-4-X members, most new locations for extended development lie in field extensions that contain sparsely drilled areas in the north and northeast parts of the LL-652 area (figs. 27 and 28). However, other targets include the system of reverse faults in the west part of compartment V, as well as the south limb of the field in compartment VII (see fig. 7). The east and south-central parts of compartment V contain areas in which delta-front and distributary-channel sandstones of the C-3-X and C-4-X members have been incompletely contacted. Most extended-development locations in the C-5-X member lie in compartments I, II, and III, whereas only six are targeted in compartment VII, principally along the zone of reverse faults. In contrast, virtually all extended-development locations in the C-6-X member lie in the central structural block and target relatively high volumes of remaining oil in delta-front sandstones.

Resource-Targeted Infill Wells

Resource-targeted (strategic infill) drilling is required to tap remaining mobile oil in uncontacted compartments of heterogeneous reservoirs. The structurally and stratigraphically complex LL-652 area has a high potential for drilling successful, off-pattern infill wells. Experience has shown (Tyler and others, 1986; Bebout and others, 1987) that strategic infill wells in mature fields are often located in parts of the reservoir that have superior reservoir quality. Typically these are the most productive areas of conventional primary production as delineated by early development wells. Optimal advanced recovery through deployment of targeted infill drilling in the LL-652 area should also focus on areas of superior reservoir quality and high productivity.

Depositional trends govern location of reservoir areas that have high amounts of remaining mobile oil. The sandstone trends are strongly linear and consistently oriented northeastward, reflecting dip-elongate, distributary-channel, and tidal-sand-ridge deposits. Although partly drained by existing wells, these sandstone-rich trends offer numerous sites for strategic infill wells. We estimate that deployment of infill wells will increase recovery efficiency by an incremental 5 percent of the OOIP.

In the C-3-X and C-4-X members 102 infill-well locations have been targeted to contact remaining mobile oil (fig. 28), and 50 locations have been targeted in the C-5-X member. These infill-well locations, targeting large volumes of remaining mobile oil, are projected to recover an average of 830,000 STB of oil in the C-3-X and C-4-X members and 500,000 STB in the C-5-X member. In total, these wells are projected to add to the LL-652 reserve base 110 MMSTB of oil produced from the C-3-X, C-4-X, and C-5-X members.

Horizontal and Inclined Wells

Opportunities exist for contacting remaining oil in the high-permeability Middle C-3-X and Upper C-4-X submembers by means of 14 horizontal wells (fig. 28). In contrast to conventional vertical wells (new locations or infill wells), horizontal wells in these submembers target reservoir areas that have (1) high permeability, (2) high volumes of remaining oil, (3) high SoPhiH values, and (4) low water saturation. Moreover, these areas have been poorly developed by previous wells, and they occur in structurally simple parts of the field. Because reservoir sandstones in the Middle C-3-X and Upper C-4-X submembers lie in northeast-trending belts of distributary-channel and delta-front deposits, horizontal wells should be oriented northeast-southwest to intersect zones of maximum permeability, SoPhiH, and remaining oil. Additionally, horizontal wells can contact bypassed oil in internally heterogeneous reservoirs, such as the Upper C-4-X submember that consists of multiple sandstones interbedded with low-permeability mudstones. Complexly stratified reservoirs such as

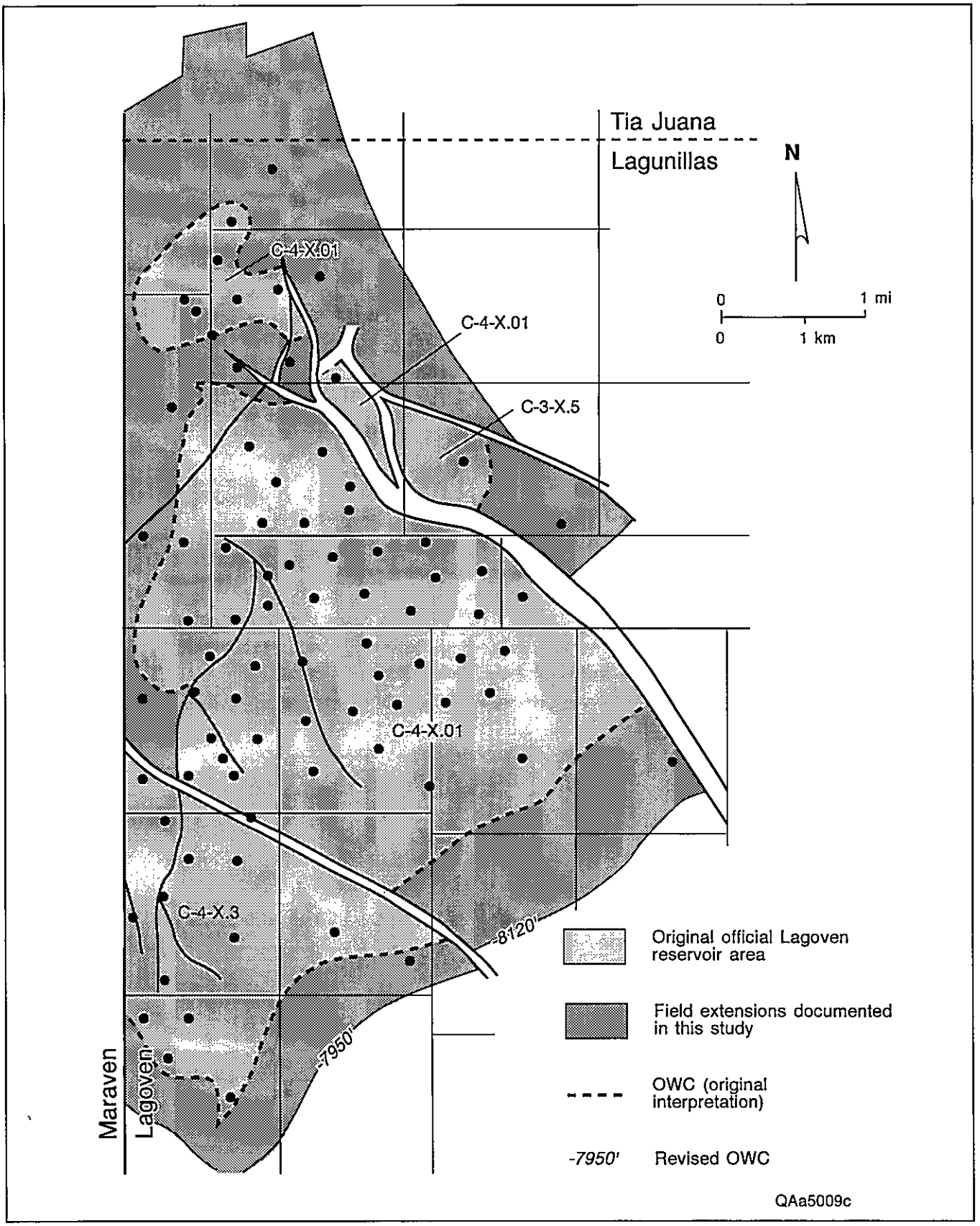


Figure 27. Field extensions in the Middle C-3-X submember. Significant volumes of remaining oil (locally >4 MMSTB) occur in the north field extension (fig. 25e).

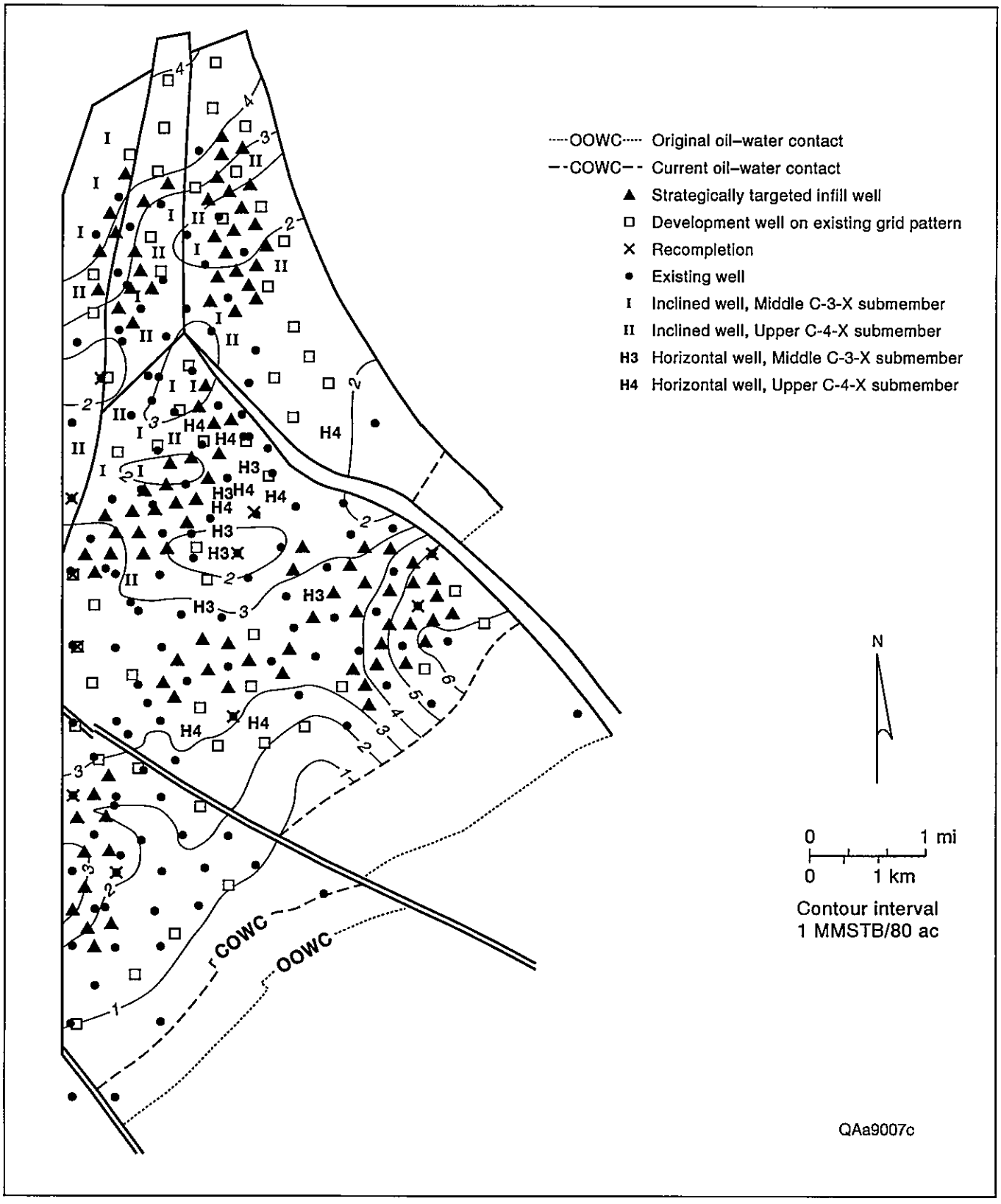


Figure 28. Map of remaining oil, Middle C-3-X submember, showing proposed new well locations, recompletions, redrilled wells, infill wells, and horizontal and inclined wells for the C-3-X and C-4-X members.

the Upper C-4-X submember contain numerous vertical-flow baffles and boundaries associated with facies changes; multiple compartments in this type of reservoir can be drained simultaneously by a single horizontal borehole (Finley and others, 1990).

Twenty-three inclined wells are recommended to target the Middle C-3-X and Upper C-4-X submembers in areas of steeply dipping strata in the north part of the LL-652 area (fig. 28). These inclined wells are projected to contact areas of (1) high permeability, (2) high volumes of remaining oil, (3) high SoPhiH values, (4) low water saturation, and (5) poor development. In contrast to horizontal wells, inclined wells are not limited by structural complexity. Because strata adjacent to the reverse faults commonly dip at high angles, inclined wells will be necessary to contact remaining oil (fig. 28). Fifteen additional inclined wells are recommended in the three north structural compartments (I, II, and III in fig. 7). Seven of these wells are targeted for the Middle C-3-X submember, and eight are selected for the Upper C-4-X submember. Because SoPhiH and net-pay values are uniformly high and water-saturation values are pervasively low in the north part of the LL-652 area, the main criteria used in selecting inclined-well locations were areas of steeply dipping strata that have high permeability values at a relative distance from previously producing wells.

Secondary Recovery

A pilot waterflood (fig. 29) in the complexly stratified Upper C-4-X submember in the east-central structural compartment V (fig. 7) could recover as much as an additional 20 percent of the OOIP in the form of unswept mobile oil locally occurring in poorly drained reservoir compartments. Sandstones in the Upper C-4-X submember were deposited in northeast-trending deltaic progradational wedges in a net retrogradational sequence, resulting in the lower part of the sequence containing thick (commonly >30 ft [>9 m]) distributary-channel and lower delta-plain sandstones and the upper part containing numerous but thin (commonly 5 to 15 ft [1.5 to 4.5 m]) delta-front sandstones. As a result of strong tidal processes, the deltaic sands were reworked into narrow (600 to 1,500 ft [183 to 457 m]), northeast-trending, dip-parallel belts (fig. 21) that may control anisotropic reservoir drainage patterns. The pilot area covers about 4.6 mi^2 (~12 km^2), has 18 wells, and was selected because (1) initial geologic studies suggest that lateral discontinuities exist in the pilot area, (2) the reservoir pressure in the pilot area is declining faster than in other reservoirs, and (3) it lies in a structurally simple area. The pilot study area lies on the north limb of a rapidly north-to-northwest-advancing zone of water encroachment that may be halted or slowed by a relatively shaly area defined by a northeast-trending band of less than 70 ft (<21.3 m) of net sandstone that bisects the pilot study area (fig. 29). The project would be expanded beyond the pilot area to include the entire fault block, creating a larger area in which different water-injection patterns could be tested.

The potential of secondary recovery for adding to the LL-652 reserve base could be quantified by means of a detailed simulation exercise. However, an indication of the volume of reserves that may be added can be gained by comparing it with that of analogous reservoirs in Texas. Fluvial-deltaic reservoirs under secondary recovery in Texas have recovery efficiencies that average 40 percent (Galloway and others, 1983). These reservoirs are typically more densely drilled than the LL-652 area, having 20- to 40-acre well spacings as compared with the 80-acre spacing in the LL-652 area. Styles of reservoir architecture also differ. This comparison suggests, however, that as much as 20 percent of the OOIP could potentially be added to the LL-652 reserve base by deploying secondary-recovery technology (fig. 26). More than 460 MMSTB of oil is the possible reward for waterflooding the LL-652 area.

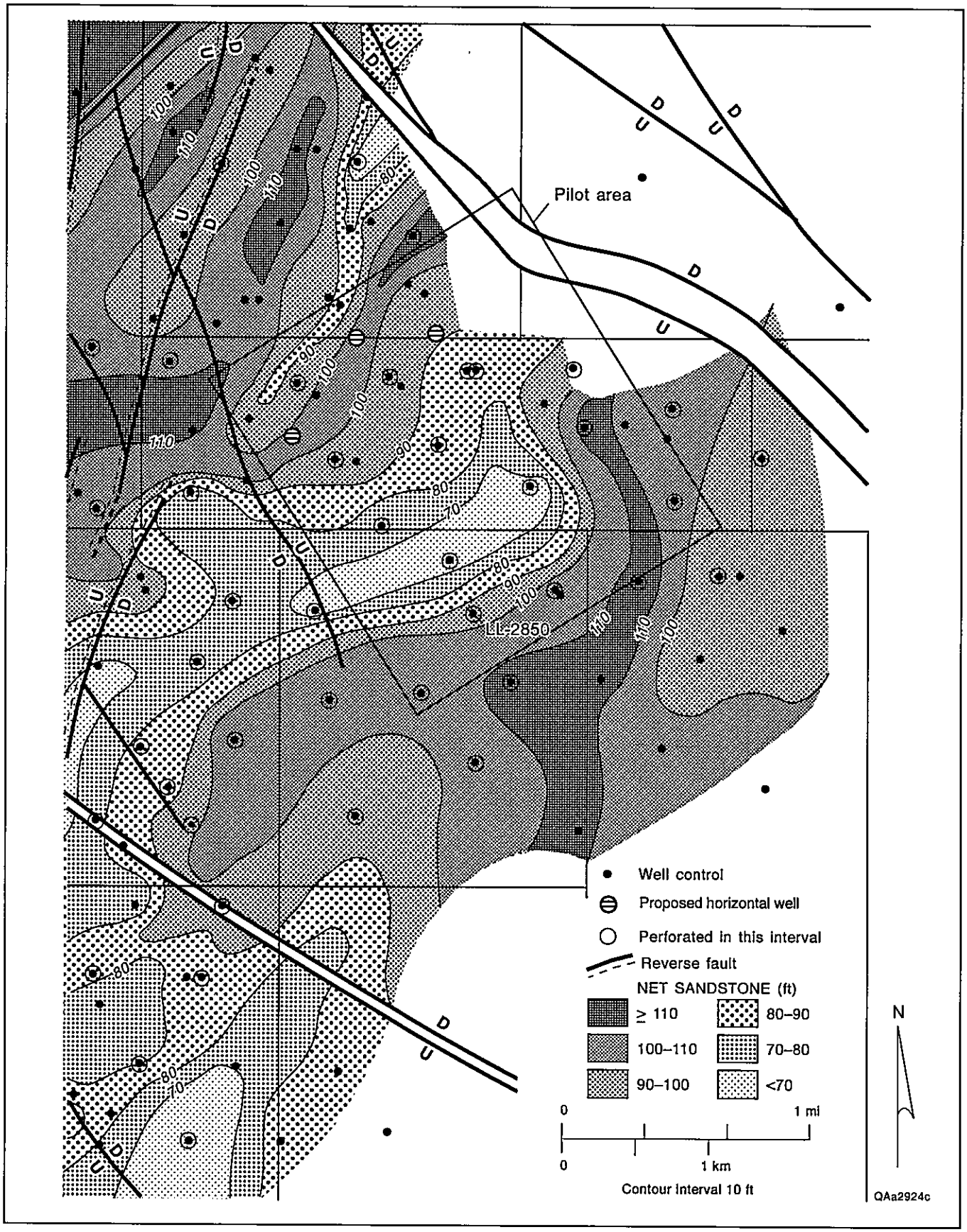


Figure 29. Net-sandstone map, Upper C-4-X submember, east part of field, showing pilot waterflood area. Proposed locations of horizontal wells also shown.

Conclusions

Poorly drained or undrained reservoir compartments in the LL-652 area are defined by a combination of structure and depositional facies geometry. The complex, multistage tectonic history of Lake Maracaibo has created many structural compartments between faults of different ages. Sandstone-body trends, as a result of the tide-dominated deltaic depositional system, are linear, parallel, and consistently oriented northeastward, imparting a preferred pathway for reservoir drainage. Because the sandstone bodies are narrow—their dimensions are typically less than the distance between wells (1,968 ft [600 m])—and are bounded laterally by low-permeability mudstones, they contain uncontacted oil that can be produced by means of cost-effective, geologically based recovery strategies.

The LL-652 resource base has been increased substantially as a result of this study. Rigorously established field limits, together with careful petrophysical analysis, have documented the OOIP resource to be 2.3 BSTB. Extended development by means of continued pattern infill can increase reserves from 127 to 302 MMSTB. Substantial volumes of oil (923 MMSTB) will, however, remain in the LL-652 area after proved and extended-development reserves have been recovered. This mobile oil will be targeted for recovery by deploying 102 geologically optimized infill wells that are projected to recover 116 MMSTB of oil. An additional 14 geologically targeted horizontal and 23 inclined wells will contact undeveloped areas of projected high permeability in the C-3-X and C-4-X submembers.

Acknowledgments

Research done on this report was conducted for and funded by Lagoven, S.A., and was assisted by Pedro Gamboa, Mohan Javalagi, Senira Kattah, Ronald Johns, Hong Liu Zheng, Doug Dawson, Danilo Boscan, and Erika Ibarra. The manuscript benefited from the reviews of Tucker F. Hentz, Lee E. McRae, Steven J. Seni, Paul R. Knox, and H. Scott Hamlin. Discussions with Bruno C. Vendeville and Stephen E. Laubach, who reviewed the structural interpretation, were extremely helpful.

Figures were drafted by Michele Bailey, William C. Bergquist, Randy Hitt, Susan Krepps, Joel L. Lardon, Patrice A. Porter, Kerza A. Prewitt, Jana S. Robinson, Maria E. Saenz, and Tari Weaver, under the supervision of Richard L. Dillon and Joel L. Lardon. Editing was by Lana Dieterich. Word processing was by Susan Lloyd. Margaret L. Evans designed the report, and Tucker F. Hentz was the technical editor. Text photography was by David M. Stephens.

References

Allen, G. P., and Posamentier, H. W., 1993, Sequence stratigraphy and facies model of an incised valley fill: the Gironde Estuary, France: Journal of Sedimentary Petrology, v. 63, no. 3, p. 378–391.

Asquith, G. B., 1990, Log evaluation of shaly sandstones: a practical guide: American Association of Petroleum Geologists, Continued Education Course Notes Series No. 31, 59 p.

Beard, D. C., and Weyl, P. K., 1973, Influence of texture on porosity and permeability of unconsolidated sand: American Association of Petroleum Geologists Bulletin, v. 57, no. 2, p. 349–369.

Bebout, D. G., Lucia, F. J., Hocott, C. R., Fogg, G. E., and Vander Stoep, G. W., 1987, Characterization of the Grayburg reservoir, University Lands Dune field, Crane County, Texas: The University of Texas at Austin, Bureau

of Economic Geology Report of Investigations No. 168, 98 p.

Bot, P., and Perdomo, J. L., 1987, Análisis sismoestratigráfico del Eoceno y evolución tectónica en la Cuenca del Lago de Maracaibo: Caracas, Lagoven, S.A., Internal Report, 98 p.

de Mowbray, Tessa, and Visser, M. J., 1984, Reactivation surfaces in subtidal channel deposits, Oosterschelde, southwest Netherlands: Journal of Sedimentary Petrology, v. 54, no. 3, p. 811–824.

Eschard, R., Ravenne, C., Houel, P., and Knox, R., 1991, Three-dimensional reservoir architecture of a valley-fill sequence and a deltaic aggradational sequence: influences of minor relative sea-level variations, *in* Miall, A. D., and Tyler, Noel, eds., The three-dimensional facies architecture of terrigenous clastic sediments and its implications for hydrocarbon discovery and recovery: SEPM (Society for Sedimentary Geology), v. 3, Concepts in Sedimentology and Paleontology, p. 133–147.

Finley, R. J., Laubach, S. E., Tyler, Noel, and Holtz, M. H., 1990, Opportunities for horizontal drilling in Texas: The University of Texas at Austin, Bureau of Economic Geology Geological Circular 90-2, 32 p.

Fisher, W. L., 1987, Can the U.S. oil and gas resource base support sustained production?: Science, v. 236, p. 1631–1636.

Folk, R. L., 1980, Petrology of sedimentary rocks: Austin, Texas, Hemphill, 182 p.

Galloway, W. E., Ewing, T. E., Garrett, C. M., Jr., Tyler, Noel, and Bebout, D. G., 1983, Atlas of major Texas oil reservoirs: The University of Texas at Austin, Bureau of Economic Geology, 139 p.

Gonzalez de Juana, C., Iturraide, J., and Picard, X., 1980, Geología de Venezuela y sus cuencas petróliferas: Caracas, Foninves, 1031 p.

Graves, G. R., Adams, G. E., Guzman, J. I., Seijas, F., Petzal, C., Furrer, M., and Meyer, R., 1987, Estudio del Eoceno del Lago de Maracaibo, parte norte y este: Caracas, Lagoven, S.A., Internal Report, 197 p.

Herron, M. M., 1987, Estimating the intrinsic permeability of clastic sediments from geochemical data, *in* Transactions, Society of Professional Well Log Analysts, 28th Annual Logging Symposium, paper HH.

Johnson, W. L., and Linke, W. A., 1978, Some practical applications to improve formation evaluation of sandstones in Mackenzie Delta, *in* Transactions, Society of Professional Well Log Analysts, 19th Annual Logging Symposium, paper C.

Klein, G. de V., 1970, Depositional and dispersal dynamics of intertidal sand bars: Journal of Sedimentary Petrology, v. 40, p. 1095–1127.

Lugo, Jairo, 1991, Cretaceous to Neogene tectonic control on sedimentation: Maracaibo Basin, Venezuela: The University of Texas at Austin, Ph.D. dissertation, 219 p.

Maguregui, J. A., 1990, Evolution and reservoir properties of middle Eocene tide-dominated deltaic sandstones in eastern Lagunillas field, Maracaibo Basin, Venezuela: The University of Texas at Austin, Master's thesis, 171 p.

Maguregui, J. A., and Tyler, Noel, 1991, Evolution of middle Eocene tide-dominated deltaic sandstones, Lagunillas field, Maracaibo Basin, western Venezuela, *in* Miall, A. D., and Tyler, Noel, eds., The three-dimensional facies architecture of terrigenous clastic sediments and its implications for hydrocarbon discovery and recovery: SEPM (Society for Sedimentary Geology), v. 3, Concepts in Sedimentology and Paleontology, p. 233–244.

Meckel, L. D., 1975, Holocene sand bodies in the Colorado delta area, northern Gulf of California, *in* Broussard, M. L., ed., Deltas: models for exploration: Houston Geological Society, p. 239–265.

Neasham, J. W., 1977, The morphology of dispersed clay in sandstone reservoirs and its effect on sandstone shaliness, pore space and fluid flow properties: Society of Petroleum Engineers Paper No. 6858, 8 p.

Off, Theodore, 1963, Rhythmic linear sand bodies caused by tidal currents: American Association of Petroleum Geologists Bulletin, v. 47, no. 2, p. 324–341.

Reineck, H. E., and Singh, I. B., 1973, Depositional sedimentary environments: with reference to terrigenous clastics: Berlin, Springer-Verlag, 439 p.

Reineck, H. E., and Wunderlich, F., 1968, Classification and origin of flaser and lenticular bedding: Sedimentology, v. 11, p. 99–104.

Reinson, G. E., Clark, J. E., and Foscolos, A. E., 1988, Reservoir geology of Crystal–Viking field, Lower Cretaceous estuarine tidal channel-bay complex, South-Central Alberta: American Association of Petroleum Geologists Bulletin, v. 72, no. 10, p. 1270–1294.

Terra Science, 1993, T log for advanced well log analysis, *in* Manual for TerraStation: Denver, Terra Science Inc., v. 5.4, 189 p.

Tye, R. S., and Coleman, J. M., 1989, Depositional processes and stratigraphy of fluvially dominated lacustrine deltas: Mississippi delta plain: Journal of Sedimentary Petrology, v. 59, no. 6, p. 973–996.

Tyler, Noel, 1988, New oil from old fields: Geotimes, v. 33, p. 8–10.

Tyler, Noel, Ambrose, W. A., Dutton, S. P., Wang, F. P., Yeh, J. S., Ferrer, Eulise, Padron, Antonio, and Carrasquel, Williams, 1994, Characterization of lower Eocene reservoirs in the LL-652 area, Lagunillas field: The University of Texas at Austin, Bureau of Economic Geology, final report prepared for Lagoven, S.A., 425 p.

Tyler, Noel, Galloway, W. E., Garrett, C. M., Jr., and Ewing, T. E., 1984, Oil accumulation, production characteristics, and targets for additional recovery in major oil reservoirs of Texas: The University of Texas at Austin, Bureau of Economic Geology Geological Circular No. 84-2, 31 p.

Tyler, Noel, Gholston, J. C., and Ambrose, W. A., 1986, Genetic stratigraphy and oil recovery in an Upper Cretaceous wave-dominated deltaic reservoir, Big Wells (San Miguel) field, South Texas: The University of Texas at Austin, Bureau of Economic Geology Report of Investigations No. 153, 38 p.

Walton, W. M., 1967, The informal units of the subsurface Eocene: Asociación Venezolana de Geología, Minería y Petróleo Boletín, v. 10, no. 1, p. 21–30.

Zambrano, E., Vasquez, E., Duval, B., Latreille, M., and Confineres, B., 1972, Paleogeographic and petroleum synthesis of western Venezuela: Paris, Editions Technip, 62 p.